

Supporting Information for

**Suppressing Photo-oxidation of Non-fullerene Acceptors and Their Blends
in Organic Solar Cells by Exploring Material Design and Employing
Friendly Stabilizers**

Jing Guo,^a Yao Wu,^a Rui Sun,^a Wei Wang,^a Jie Guo,^a Qiang Wu,^a Xiaofeng Tang,^b Chenkai Sun,^c Zhenghui Luo,^d Kai Chang,^d Zhuohan Zhang,^e Jun Yuan,^f Tengfei Li,^g Weihua Tang,^e Erjun Zhou,^h Zuo Xiao,ⁱ Liming Ding,ⁱ Yingping Zou,^f Xiaowei Zhan,^g Chuluo Yang,^d Zhen Li,^d Christoph J. Brabec,^b Yongfang Li,^c Jie Min^{a*}

J. Guo, Y. Wu, R. Sun, W. Wang, J. Guo, Q. Wu, Prof. J. Min

^aThe Institute for Advanced Studies, Wuhan University, Wuhan 430072, China

E-mail: min.jie@whu.edu.cn

X. Tang, Prof. C. J. Brabec

^bInstitute of Materials for Electronics and Energy Technology (I-MEET), Friedrich-Alexander University Erlangen-Nuremberg, Martensstraße 7, 91058 Erlangen, Germany

C. Sun, Prof. Y. F. Li

^cBeijing National Laboratory for Molecular Sciences, CAS Key Laboratory of Organic Solids, Institute of Chemistry, Chinese Academy of Sciences, 100190 Beijing, China.

Z. Luo, K. Chang, Prof. C. L. Yang, Prof. Z. Li

^dHubei Key Lab on Organic and Polymeric Optoelectronic Materials, Department of Chemistry,

Wuhan University, Wuhan 430072, China

Z. Zhang, Prof. W. H. Tang

^eSchool of Chemical Engineering, Nanjing University of Science and Technology, Nanjing 210094, China.

J. Yuan, Prof. Y. P. Zou

^fCollege of Chemistry and Chemical Engineering, Central South University, Changsha 410083, China.

T. Li, Prof. X. W. Zhan,

^gDepartment of Materials Science and Engineering, College of Engineering, Key Laboratory of Polymer Chemistry and Physics of Ministry of Education, Peking University, Beijing 100871, China

Prof. E. J. Zhou,

^hHenan Institutes of Advanced Technology, Zhengzhou University, Zhengzhou 450003, China.

Prof. Z. Xiao, Prof. L. Ding

ⁱCenter for Excellence in Nanoscience (CAS), Key Laboratory of Nanosystem and Hierarchical Fabrication (CAS), National Center for Nanoscience and Technology, Beijing 100190, China.

Experimental Section

Materials: PTQ10 and PDINO were provided by Yongfang Li's group. J71 and P3HT were

purchased from Solarmer Materials Inc. The provider of non-fullerene acceptors and fullerene derivatives were compiled in table S5. The stabilization additives including 2,2,6,6-Tetramethylpiperidinoxy (S1), 2,6-di-*t*-butyl-4-methylphenol (S2), Tris(2,4-di-*tert*-butylphenyl)phosphite (S3), Pentaerythrityl tetrakis[3-(3,5-di-*tert*-butyl-4-hydroxyphenyl)propionate] (S4), Zinc dibutyldithiocarbamate (S5) and Nickel dibutyldithiocarbamate (S6) were purchased from Heowns Biochem Technologies LLC. Zinc acetate dehydrate, 2-methoxyethanol, and ethanolamine were provided by Sigma Aldrich. Solvents (chloroform and methanol) were dried and distilled from appropriate drying agents prior to use.

Device Fabrications and Characterization: The conventional devices were fabricated with a structure of ITO/PEDOT: PSS (40 nm)/active layer/PDINO/Al. Patterned ITO substrates were cleaned with methylbenzene, deionized water, acetone and isopropyl alcohol in an ultrasonic bath for 10 min each. After drying, a thin layer of PEDOT: PSS was deposited through spin-coating on ITO-coated glass from a PEDOT: PSS aqueous solution (Xi'an Polymer Light Technology Corp 4083) at 4,000 rpm and dried subsequently at 150 °C for 15 min in air. ZnO precursor solution (109.8 mg of zinc acetate dehydrate dissolved in 1 mL of 2-methoxyethanol and 30.2 μ L of ethanolamine) was spin-coated on plasma treated ITO substrates at 4000 rpm for 60s, following by thermal annealing at 200 °C for 30 minutes. Besides, for the devices using MoO₃ as the interlayer, 10 nm of MoO₃ was thermally evaporated on the ITO coated glasses under a vacuum of $\sim 5 \times 10^{-6}$ mbar. Then the active layer (app. 100 nm) was spin-coated in a N₂-filled glovebox from polymers:acceptors blend solution (J71:ITIC, IT-4F, IDIC, O-IDTBR, PC₇₁BM and PBDB-T:ITIC, ITCC, IDIC, O-IDTBR) in chloroform (1:1, wt%; 12 mg mL⁻¹) onto the PEDOT: PSS(MoO₃, and ZnO layer for J71:ITIC bend). The spin speed was adjusted to different blend solutions. For the layer-by-layer (LBL) structure device, donor and acceptor materials was dissolved in chloroform solution separately with a concentration of 12mg mL⁻¹. Firstly, donor was spin-coated on PEDOT:PSS layer to form a front layer, then acceptor was also spin-coated onto the surfaces of donor layers with same rotating speeds of 2500rpm. After that, the active layers were annealed at 150 °C for 10 min or there's no anneal only for testing of antioxidation additives. Then methanol solution of PDINO at a concentration of 1.0 mgml⁻¹

¹ was spin-coated onto the active layer at 3,000 rpm for 30s. To complete the fabrication of the devices, 100 nm of Al (or 10nm of MoO₃ and 100nm of silver for ZnO device) were thermally evaporated through a mask under a vacuum of $\sim 5 \times 10^{-6}$ mbar. The active area of the devices was 4 mm². The devices were encapsulated by glass slides using epoxy in nitrogen filled glovebox prior to measurement. Here exposure prior to electron transport layer and electrode deposition allowed the investigations to focus on the underlying kinetics of the polymers:acceptors photo-oxidation independent of the mechanisms of oxidation process in electrodes. The current-voltage characteristics of the solar cells were measured under AM 1.5G irradiation on an Enli Solar simulator (100 mW cm⁻²). Before each test, the solar simulator was calibrated with a standard single-crystal Si solar cell (made by Enli Technology Co., Ltd., Taiwan, calibrated by The National Institute of Metrology (NIM) of China). Photo-oxidation of entire solar cells were illuminated under the solar simulator and tracked by periodically measuring the *J-V* curves. The temperature of the devices was monitored and hold at below 40°C.

Photo-oxidation Degradation: Photo-oxidation of thirty-five acceptor films degradation procedure was performed on quartz substrate cleaned as mentioned above. Typical concentrations of the acceptors studied were 12-18 mg/mL, followed by annealing at 150 °C for 10 min and then illuminated under AM 1.5G in dry air without filters (relative humidity \approx 30%) for different periods of time mentioned in the main text. To eliminate the side effect from photo-induced elevation of temperature on the film. The quartz substrate with active film was placed on the metal plate and blew by the electric fan (below 30°C). For testing of antioxidation, the antioxidation additives were dissolved in chloroform ahead of time with a concentration of 0.03-2.4mg/mL, forming well-mixed solvent as the one used for dissolving the organic materials, Preparation of film was conducted on the quartz substrate by spin-coating without anneal. The photo-oxidation of film was congruity with common method. Degraded ITIC for selective degradation study was prepared by dissolving ITIC (32 mg) in chlorobenzene (CB) (2.6 mL) in a 15 mL vial with stir speed of 300 rpm in a nitrogen filled glovebox for at least 12 hours. The vial of ITIC solution was then filled with air and degraded under AM 1.5G

illumination with stir speed of 100 rpm for 72 hours in dry air.

Material and Film Characterizations: Atomic Force Microscopy (AFM) images were obtained by using Nano Wizard 4 atomic force microscopy (JPK Inc. Germany) in Qi mode to observe the surface morphologies of degraded blend films deposited on glass substrates. Film absorption was characterized periodically by a Perkin Elmer Lambda-365 absorption spectrometer with the spectrum ranging from 300 nm to 1100 nm and adjusted according to different materials. FTIR spectra were measured on a Nicolet 5700 infrared spectrometer with wavenumber ranging from 400 to 4000 cm^{-1} . Photoluminescence (PL) data were collected using a Zolix Flex One Spectrometer equipped with 405 nm laser.

XPS data were obtained using a Thermo Fisher Scientific ESCALAB250Xi (Thermo Fisher Scientific, UK) using a monochromated Al α source. All spectra were recorded using a charge neutralizer to remove differential charging. The main carbon peak is charge referenced to 284.5 eV.

Mass spectra (MALDI-TOF-MS) were determined using a Bruker BIFLEX III Mass Spectrometer. High resolution mass spectra (HRMS) were determined on a Bruker Daltonics Inc. BIFLEX III MALDI-TOF or a Waters micromass GCT Mass Spectrometer.

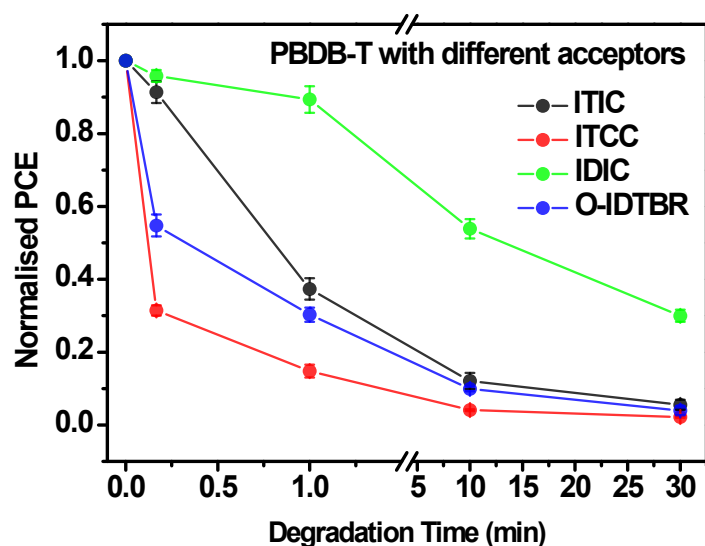


Figure S1. Normalized PCEs of PBDB-T devices based on degraded BHJ blends as a function of illumination time.

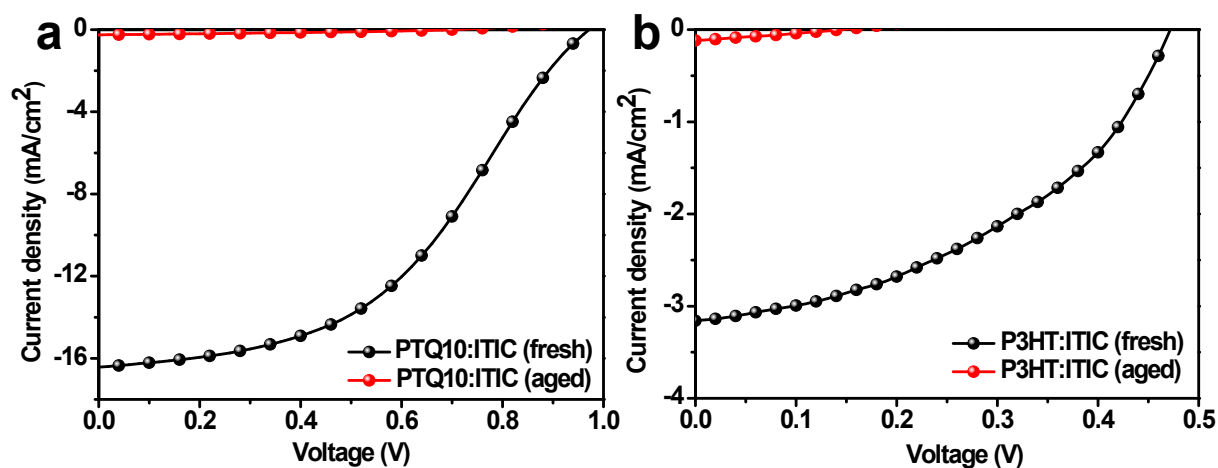


Figure S2. *J-V* characteristics of (a) PTQ10:ITIC and (b) P3HT:ITIC devices with and without 30 minutes under simulated AM 1.5G illumination in air (the films were exposed to solar simulated light prior to back contact deposition).

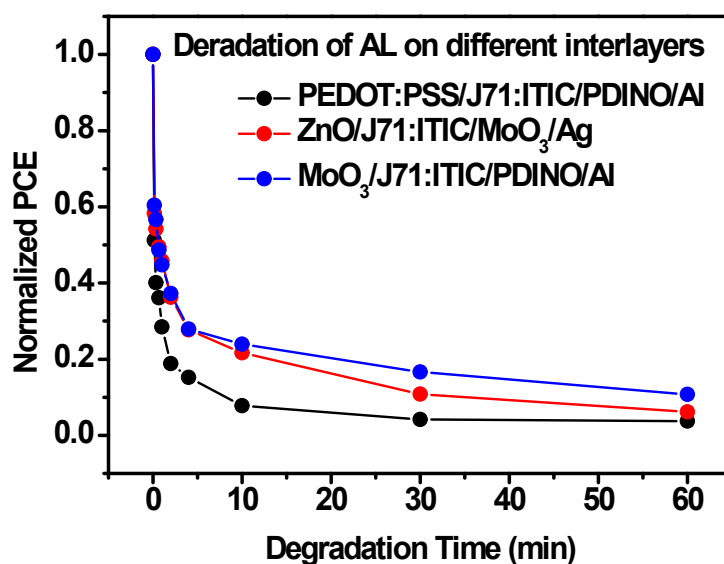


Figure S3. Normalized PCE of J71:ITIC devices with active layers degrading on PEDOT:PSS, MoO₃, and ZnO interlayers.

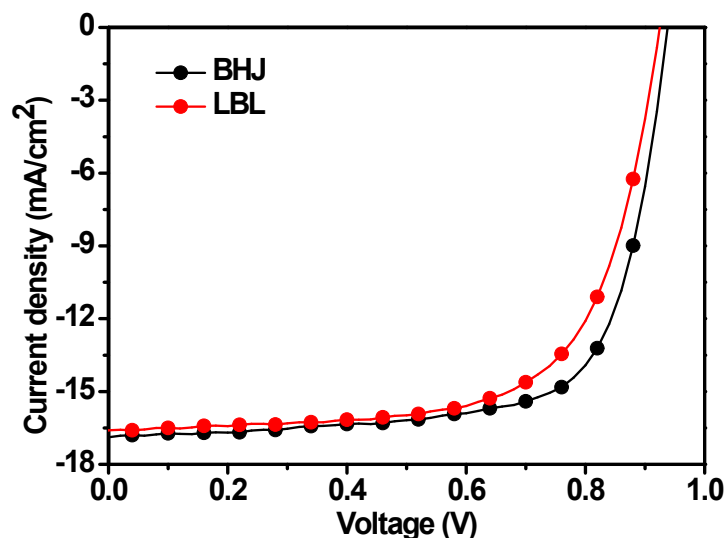


Figure S4. J - V characteristic of J71:ITIC devices based on BHJ and LbL films measured under simulated AM1.5G illumination.

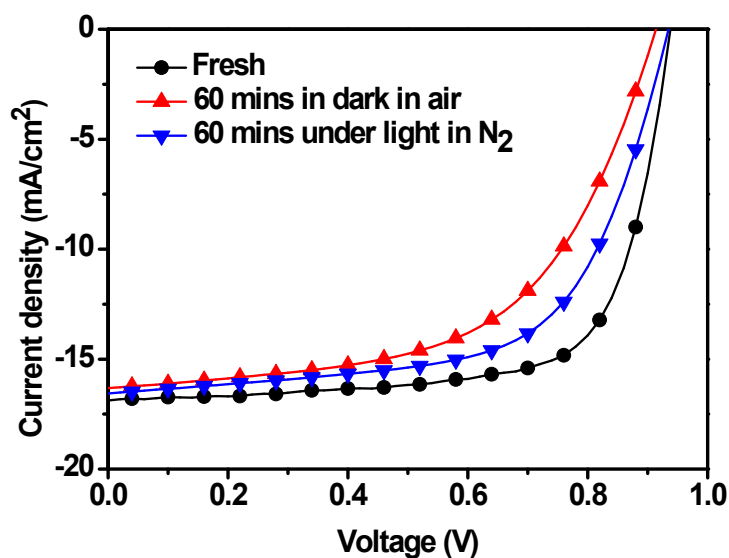


Figure S5. J - V characteristic of J71:ITIC devices exposed to air for 60 minutes in the dark and illuminated under simulated AM1.5G illumination for 60 minutes in N_2 .

Table S1. Summary of device parameters of J71:ITIC devices exposed to air for 60 minutes in the dark and illuminated under simulated AM1.5G illumination for 60 minutes in N_2 .

Film degradation condition	V_{OC} [V]	J_{SC} [mA/cm ²]	FF [%]	PCE [%]	PCE ^a [%]
Fresh	0.938	16.88	71.12	11.26	11.15
60 mins in dark in air	0.920	16.31	57.87	8.68	8.59
60 mins under simulated AM1.5G illumination in N_2	0.934	16.56	62.55	9.68	9.39

^aThe values in square bracket are the average PCE obtained from six devices.

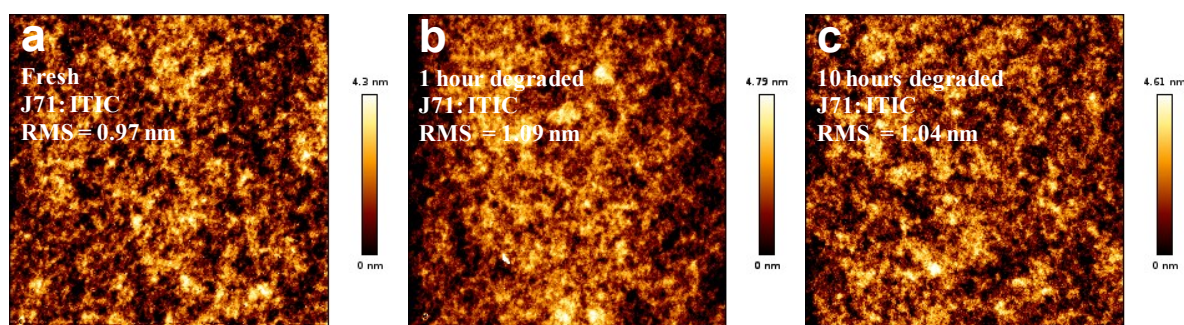


Figure S6. Qi mode AFM height images and average roughness analysis of (a) fresh J71:ITIC blend films (RMS = 0.97nm); J71:ITIC blend films degraded under one sun in dry air for (b) 1 hour (RMS = 1.09 nm) and (c) 10 hours (RMS = 1.04 nm), respectively.

Table S2. Summary of device parameters of ITO/PEDOT:PSS/J71: ITIC/PDINO/Al devices with different degradation times under simulated AM1.5G illumination in air, before top electrode deposition.

Film degradation time[mins]	V_{OC} [V]	J_{SC} [mA/cm ²]	FF [%]	PCE [%]	PCE ^a [%]
0	0.938	16.88	71.12	11.26	11.15
1/6	0.902	12.86	45.44	5.27	5.20
1	0.883	8.75	41.91	3.24	3.16
4	0.854	5.34	40.94	1.87	1.83
10	0.842	3.93	40.32	1.33	1.30
30	0.825	2.52	40.49	0.84	0.83

^aThe values in square bracket are the average PCE obtained from 6 devices.

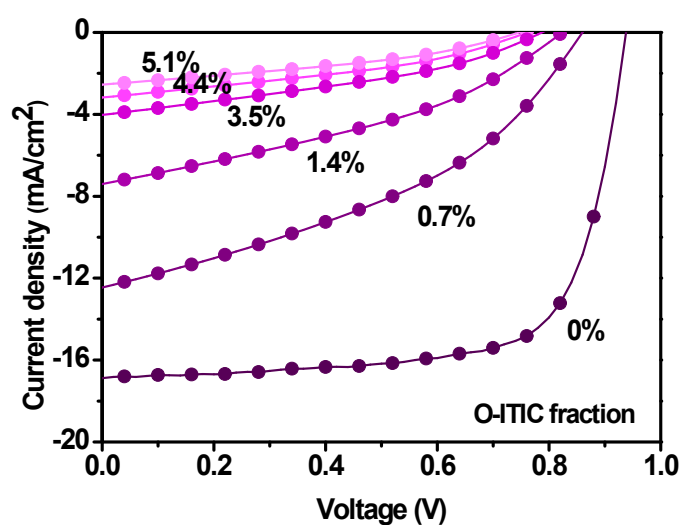


Figure S7. J - V characteristic of the solar cells based on J71:ITIC:O-ITIC blend doped with different fractions of O-ITIC, the percentages indicating the mass fraction of O-ITIC in the

ITIC phase. In the J71:ITIC:O-ITIC solar cells, a 62% loss in device performance was observed when only 0.7% O-ITIC as the third component was added in J71:ITIC solution. Meanwhile, PCE increased to ~90% loss when the fabricated solar cell contains 3.5% O-ITIC.

Table S3. Summary of device parameters of ITO/PEDOT:PSS/J71:ITIC/PDINO/Al devices made with different fractions of degraded O-ITIC.

Fractions of degraded O-ITIC	V_{OC} [V]	J_{SC} [mA/cm ²]	FF [%]	PCE [%]	PCE ^a [%]
0	0.938	16.88	71.12	11.26	11.15
0.7%	0.859	12.45	39.35	4.21	4.18
1.4%	0.824	7.40	36.27	2.21	2.18
3.5%	0.787	4.02	35.70	1.13	1.01
4.4%	0.761	3.17	36.07	0.87	0.85
5.1%	0.747	2.55	36.09	0.68	0.66

^aThe values in square bracket are the average PCE obtained from 6 devices.

Supplementary Note 1.

Charge carrier mobility is one of the major concerns in designing organic materials. Efficient transportation and collection of the photoinduced charge carriers are reflected in high charge carrier mobility. We measured the electron only mobility of J71:ITIC blends films in different time periods by the space-charge-limited current (SCLC) method, The mobilities were obtained by taking current-voltage curves and fitting the results to a space charge limited form. The SCLC mobilities data were calculated by the following equation:

$$J_{SCL} = \frac{9}{8} \varepsilon_0 \varepsilon_r \mu \frac{V_{in}^2}{L^3} \exp\left(\frac{0.89 \times \beta}{\sqrt{L}} \sqrt{V}\right) \quad (1)$$

where J_{SCL} is the current density, ε_0 is the vacuum permittivity, ε_r is the relative dielectric constant of the active layer and the value we used here is 3, μ is the mobility of electron, L is the thickness of the active layer and V_{in} is obtained from $V_{in} = V_{app} - V_{bi} - V_s$, where V_{app} is the applied voltage, V_{bi} is the built-in voltage (0.3V), V_s is the voltage drop from the substrate's series resistance ($V_s = IR$).

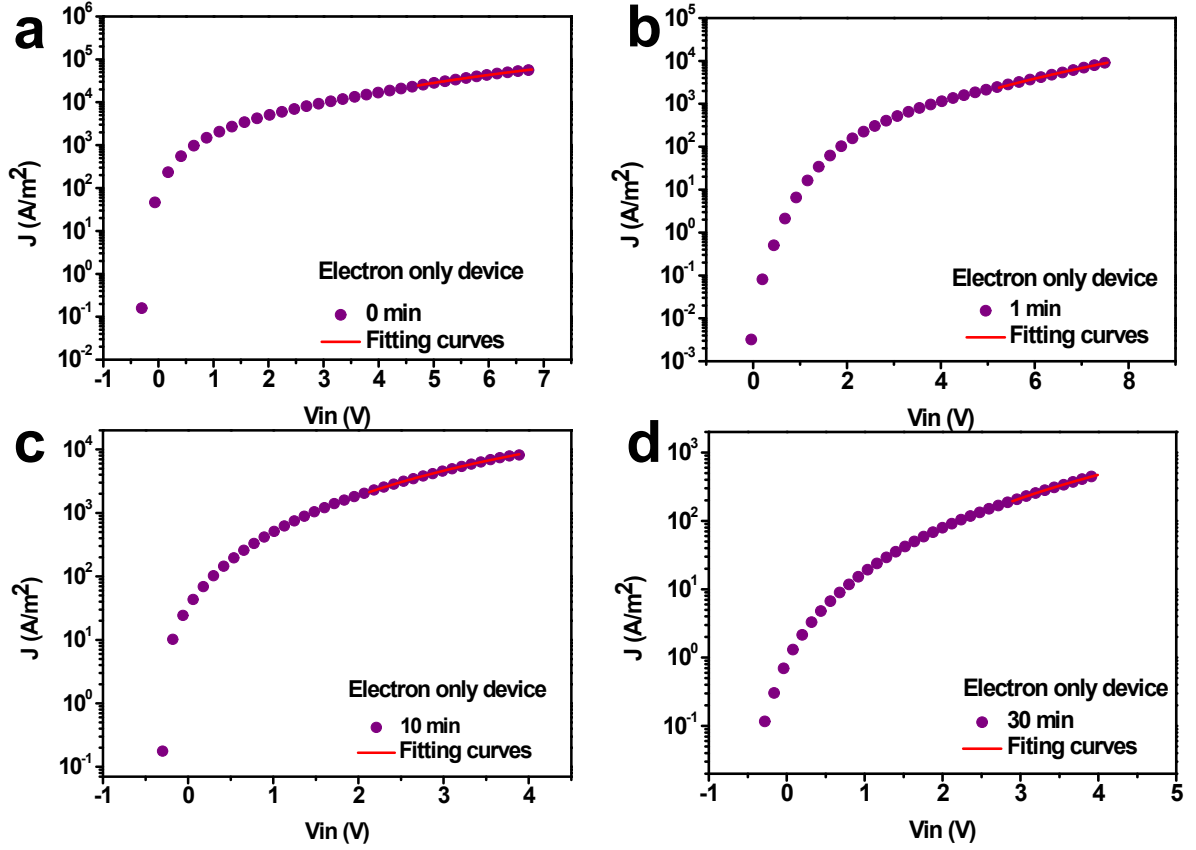


Figure S8. The Space-charge-limited(SCLC) J - V characteristics of J71:ITIC based electron-only devices exposed under AM1.5G in air for (a) 0 min, (b) 1 min, (c) 10 min and (d) 30min prior to back contact deposition (the red lines are fitting curves according to the space-charge-limited current model).

In photo-induced charge carrier extraction by linearly increasing voltage (photo-CELIV) measurement, the devices were illuminated with a 405nm laser diode and photo-generated charges were extracted using a linearly increasing voltage pulse with varied delay time. The current transients were recorded using an oscilloscope with an internal 50 Ohm resistor. From the photocurrent transient curve, the charge carrier mobility is calculated via the following equation:

$$\mu = \frac{2d^2}{3At_{max}^2 \left[1 + 0.36 \frac{\Delta j}{j(0)} \right]} \quad \text{if } \Delta j \leq j(0) \quad (2)$$

where d is the thickness of the active layer, A is the voltage rise speed $A = dU/dt$, U is the applied voltage to the device.

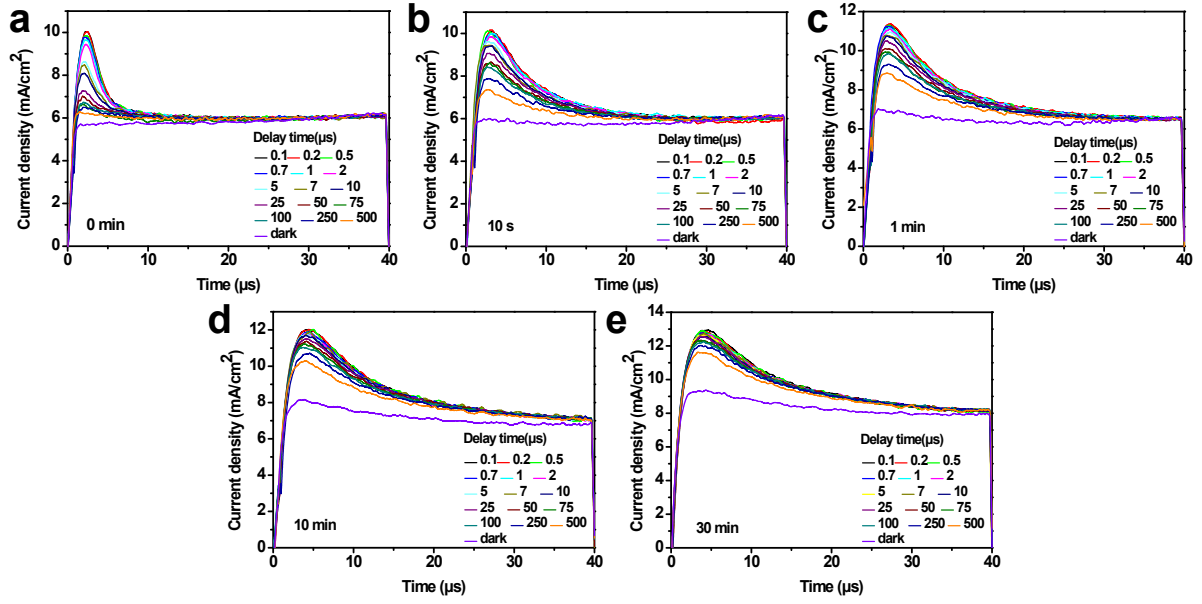


Figure S9. The photo-CELIV trace for J71:ITIC based solar cell with (a) 0 min, (b) 10s, (c) 1 min, (d) 10 min and (e) 30 min exposure time periods.

Supplementary Note 2.

To unravel the degradation recombination losses mechanisms under various time on the device performance, we studied the light intensity dependence of current density-voltage (J - V) characteristics, The J - V characteristics of the solar cells under the illumination intensities ranging from 107 to 2 mW cm⁻² were tested. The V_{oc} and light intensity (I) can be correlated by the following expression:

$$V_{oc} = \frac{E_{gap}}{q} - \frac{kT}{q} \ln\left[\frac{(1-P)\gamma N_c^2}{PG}\right] \quad (3)$$

where E_{gap} is the energy difference between the HOMO of the electron donor and the LUMO of the electron acceptor, q is the elementary charge, T is temperature in Kelvin, k is the Boltzmann constant, γ the recombination constant, P is the dissociation probability of the electron-hole pairs into free carriers, N_c the density of states in the conduction band, and G the generation rate of electron-hole pairs. This formula contains the dependence of the V_{oc} on the light intensity, as G is the only term directly proportional to the light intensity. Based on the rules, the formula predicts a slope $S = (kT/q)$ of the V_{oc} versus the natural logarithm of the

incident light intensity. In the case of 2nd order recombination, the slope of V_{oc} versus $\ln(I)$ is equal to kT/q . When trap-assisted recombination is involved, a stronger dependency of V_{oc} on the light intensity (slope larger than kT/q) is observed.

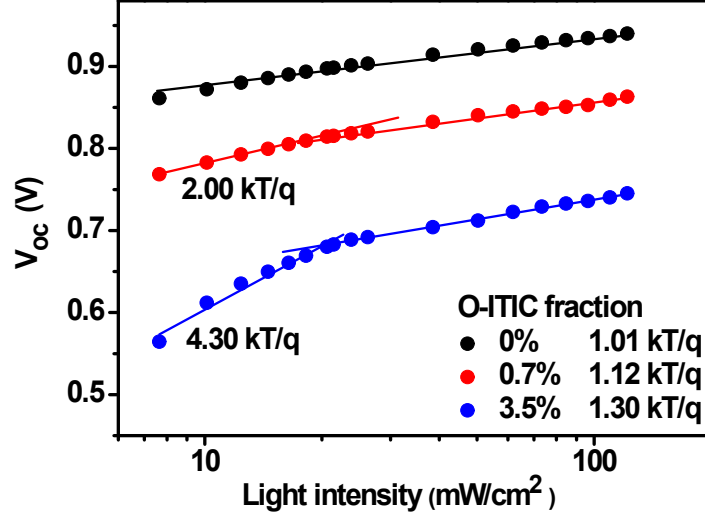


Figure S10. V_{oc} of devices with various O-ITIC fractions plotted against light intensity on a logarithmic scale.

Supplementary Note 3.

Transient photocurrent (TPC) measurement is a method for the time dependent extraction of photogenerated charge carriers and yield information about extractable charges, charge recombination and density of states. In the measurement, the sample device is in short circuit condition, the current is measured on a digital oscilloscope from the voltage across a small load resistor ($R=50 \Omega$). Using Ohms law, TPC transient is then converted into a current transient and the number of photogenerated charges can be obtained by integrating over time. The total charge carrier density under open circuit conditions $n(V_{oc})$ is calculated from:

$$n(V_{oc}) = \frac{q(V_{oc})}{edA} \quad (4)$$

where A is the area of the device. Note that this analysis assumes that the charge density Δq generated by the laser excitation is the same at the short circuit and open circuit conditions and therefore is independent of device electric fields.

Charge extraction (CE) is a simple measurement technique to allows us to quantify the amount

of extractable charge present in the device at varied light intensity corresponding to various V_{oc} , and thus provides information about the density of states. In the charge extraction experiment, the solar cell is illuminated under open-circuit conditions with a steady light irradiation, then the light is turned off and the switching the cell to short-circuit conditions (<50 ns) simultaneously, resulting in a transient current. The current extracted from the device is integrated to calculate the charge carrier density. In order to get the charge density in the active layer, n_{active} , the total charge must be reduced by the so-called geometrical charge density n_{geo} .

$$n_{active} = n_{ext.} - n_{geo.} = n_{ext.} - \frac{CV}{qdA} \quad (5)$$

where $n_{ext.}$ is the extracted charge density, C is the capacity, V is the applied voltage, q is the elementary charge, d is the thickness and A is the area of solar cell.

Transient photovoltage (TPV) is used to get information about charge carrier lifetime of a solar cell at different light intensities. The samples were held at open circuit condition and connected to the terminal of an oscilloscope. A continuously illuminated white light LED is applied to the devices to control V_{oc} . The small perturbation created by a 405nm diode laser is superimposed on background light illumination, resulting in a voltage transient with an amplitude $\Delta V_0 \ll V_{oc}$. Within the small perturbation regime, the transients were fitted to a single exponential decay, consistent with a pseudo-first-order rate equation of the form:

$$\frac{d \Delta V}{dt} \propto \frac{d \Delta n}{dt} = -k_{eff} \Delta n = -\frac{\Delta n}{\tau_{\Delta n}} \quad (6)$$

Where ΔV is the photovoltage, t is the time, Δn is the change in the density of photogenerated carriers density due to the perturbation pulse, k_{eff} is the pseudo-first order rate constant and $\tau_{\Delta n}$ is the corresponding carrier lifetime. The $\tau_{\Delta n}$ was determined from photovoltage transients recorded at different light bias from 0.2-2 suns.

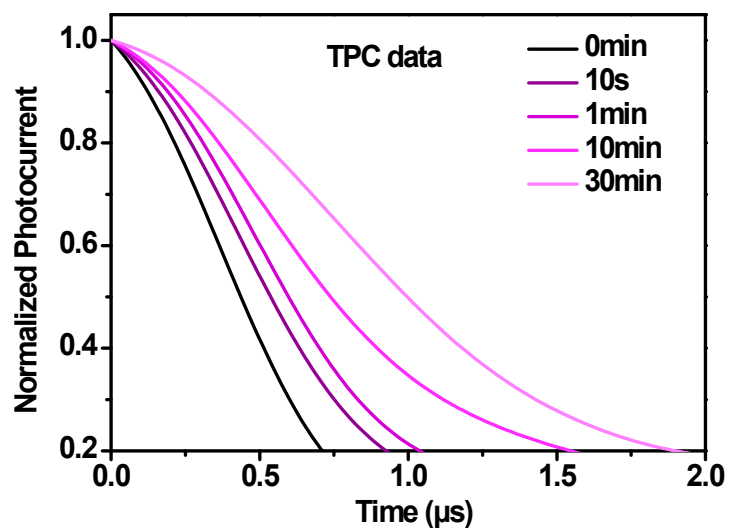


Figure S11. The TPC traces for the J71:ITIC solar cells based on their blends exposed to light and air within in different time periods.

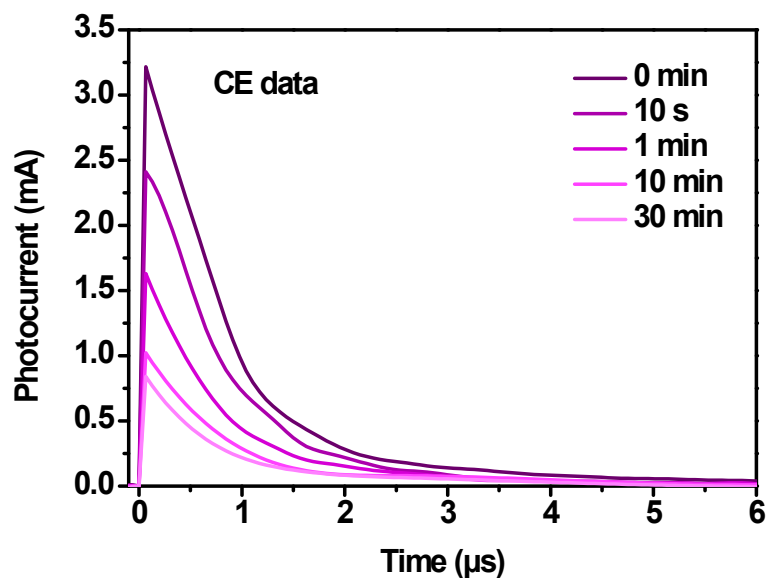


Figure S12. The CE traces for the J71:ITIC solar cells based on their blends exposed to light and air within in different time periods.

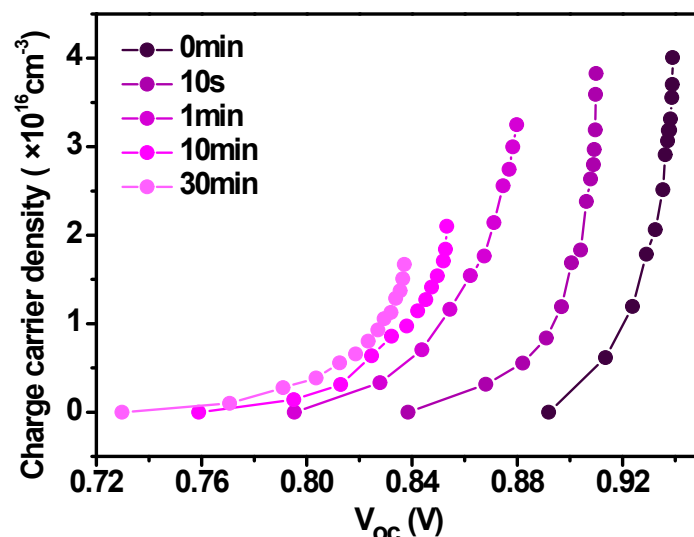


Figure S13. Charge extraction measurements of a fresh and exposed J71:ITIC solar cells show a shift in the voltage-dependent carrier density, consistent with a corresponding shift in the density of states.

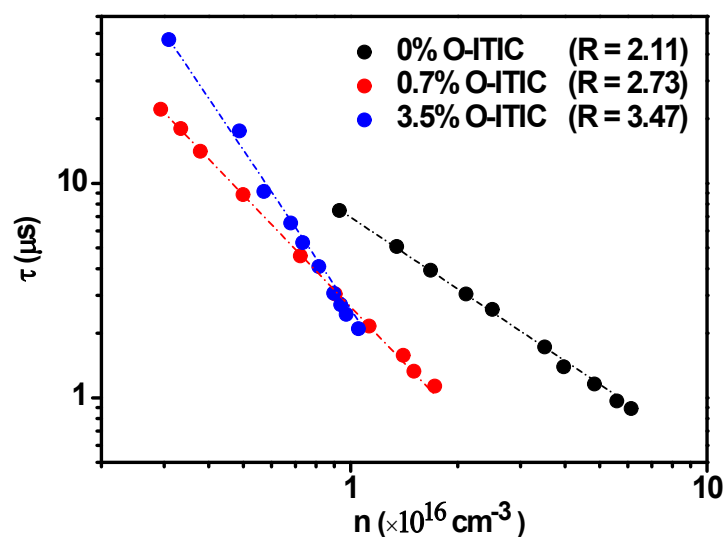


Figure S14. Charge carrier lifetime τ , obtained from TPV, as a function of charge density n , calculated from CE measurements under V_{oc} conditions (0.2 to 2 suns). The dashed lines represent linear fits of the data.

Supplementary Note 4.

Electroluminescence(EL) measurements were performed by applying an external current source through the devices powered by Keithley 2400 source meter, the emitted light was recorded with a Si CCD detector installed inside the Zolix Flex One Spectrometer.

The FTPS-EQE measurements were carried out with a modified Bruker Vertex 70 FTIR spectrometer equipped with a tungsten lamp and a quartz beam-splitter, using the solar cell as the external detector, A low noise current amplifier (Femto DLPCA-200) is used to amplify the photocurrent produced from solar cell. The output voltage of the current amplifier is fed back to the external detector port of the FTIR spectrometer.

The maximum voltage achievable in a solar cell is limited by unavoidable radiative recombination. Meanwhile, we found that the V_{oc} values of devices decreased gradually with increasing exposure time. From the ideal diode equation, the V_{oc} is determined by the ratio between short circuit current (J_{sc}) and dark saturation current (J_0), following this expression¹:

$$V_{oc} = \frac{kT}{q} \ln \left(\frac{J_{sc}}{J_0} + 1 \right) \quad (7)$$

Where k is the Boltzmann constant, T is the temperature, and q is the elementary charge. The expression for J_{sc} and J_0 are given by :

$$J_{sc} = q \cdot \int_0^{\infty} EQE_{PV}(E) \cdot \Phi_{AM1.5}(E) dE \quad (8)$$

$$J_0 = \frac{q}{EQE_{EL}} \cdot \int_0^{\infty} EQE_{PV}(E) \cdot \Phi_{BB}(E) dE \quad (9)$$

The expression for J_0 is the Rau's reciprocity relation², where EQE_{EL} is radiative quantum efficiency of the solar cell when charge carriers are injected into solar cells in dark, and Φ_{BB} is the black body spectrum.

When all the recombination is radiative (i.e. $EQE_{EL} = 1$), J_0 is minimized and V_{oc} is maximized.

$$J_0^{rad} = q \cdot \int_0^{\infty} EQE_{PV}(E) \cdot \phi_{BB}(E) dE \quad (10)$$

$$V_{oc}^{rad} = \frac{kT}{q} \ln \left(\frac{J_{sc}}{J_0^{rad}} + 1 \right) \quad (11)$$

In the Shockley-Queisser theory,³ the general quantum efficiency $EQE_{PV}^{SQ}(E)$ can be defined as follow:

$$EQE_{PV}^{SQ}(E) = 1, E \geq E_{gap}; EQE_{PV}^{SQ}(E) = 0, E < E_{gap} \quad (12)$$

Substituting general quantum efficiency $EQE_{PV}^{SQ}(E)$ (equation 12) in equation 10, then we can get the saturation current in the SQ limit, J_0^{SQ}

$$J_0^{SQ} = q \cdot \int_{E_{gap}}^{\infty} EQE_{PV}^{SQ}(E) dE = q \cdot \int_{E_{gap}}^{\infty} \phi_{BB}(E) dE \quad (13)$$

In the same way, we can calculate the value of the SQ open-circuit voltage limit, V_{oc}^{SQ} , according to equation 5,

$$V_{oc}^{SQ} = \frac{kT}{q} \ln \left(\frac{J_{sc}}{J_0^{SQ}} + 1 \right) \quad (14)$$

Therefore, we can calculate the voltage loss of radiative recombination below the gap, $\Delta V_{oc}^{rad, below gap}$

$$\Delta V_{oc}^{rad, below gap} = V_{oc}^{SQ} - V_{oc}^{rad} \quad (15)$$

The voltage loss due to non-radiative recombination, $\Delta V_{oc}^{non-rad}$, can be rewritten as

$$\Delta V_{oc}^{non-rad} = V_{oc}^{rad} - V_{oc} \quad (16)$$

Based on the previous discussion⁴, we are now able to summarize the energy loss from the E_{gap} to the qV_{oc} for any type of solar cells

$$q\Delta V = \Delta E_1 + \Delta E_2 + \Delta E_3 = (E_{gap} - qV_{oc}^{SQ}) + q\Delta V_{oc}^{rad, below gap} + q\Delta V_{oc}^{non-rad} \quad (17)$$

Therefore, we can get these three terms of energy losses based on related experiments and calculations.

Besides, specification of the three sources of E_{loss} follows the following equation:

$$E_{loss} = (E_{gap} - qE_{CT}) + (q\Delta V_{rad oc}) + (q\Delta V_{non-rad oc}) = \Delta E_1 + \Delta E_2 + \Delta E_3 \quad (18)$$

To estimate the energy of the charge transport state we have performed FTPS_EQE measurements, as shown in **Figure S15**. The lower energy part of the EQE spectra (the CT state manifold) can be fitted by Marcus theory to estimate the energy of the CT state.⁵

$$EQE(E) = \frac{f}{E\sqrt{4\pi\lambda kT}} \exp\left(-\frac{(E_{ct} + \lambda - E)^2}{4\lambda kT}\right) \quad (19)$$

where k is the Boltzmann constant, T is absolute temperature, λ is the reorganization energy and f is the oscillator absorption strength, proportional to the donor/acceptor interface area.

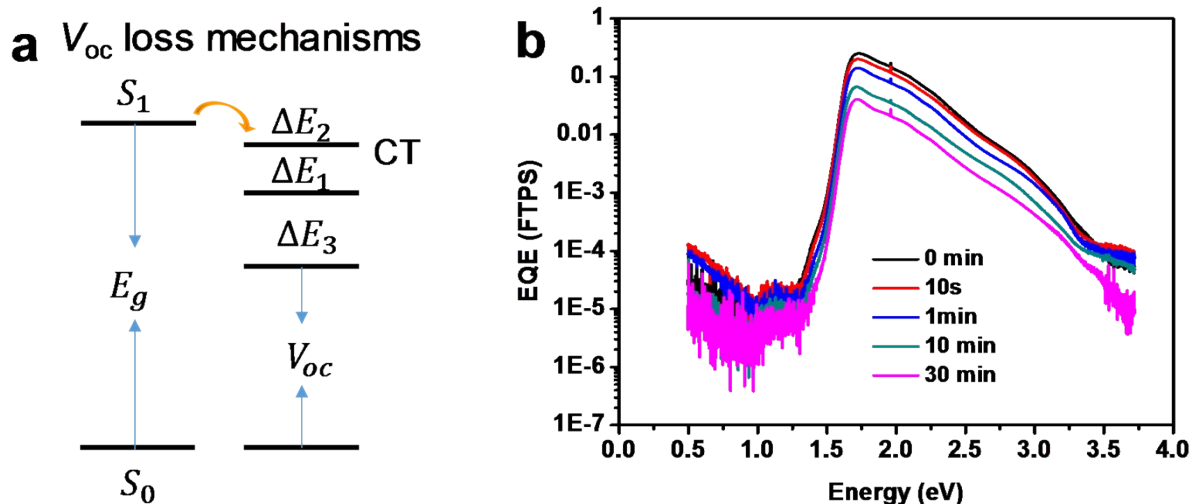


Figure S15. (a) Energy diagram showing the relationship of optical bandgap (E_{gap}), lowest singlet state (S_1), charge transfer (CT) state, V_{oc} and the three terms of energy losses for organic solar cell. (b) absolute external quantum efficiency (EQE) spectra of J71:ITIC solar cells without and with the degraded blends. The quantum efficiency data that could be directly collected on our FTSP instrument is represented by solid lines (right).

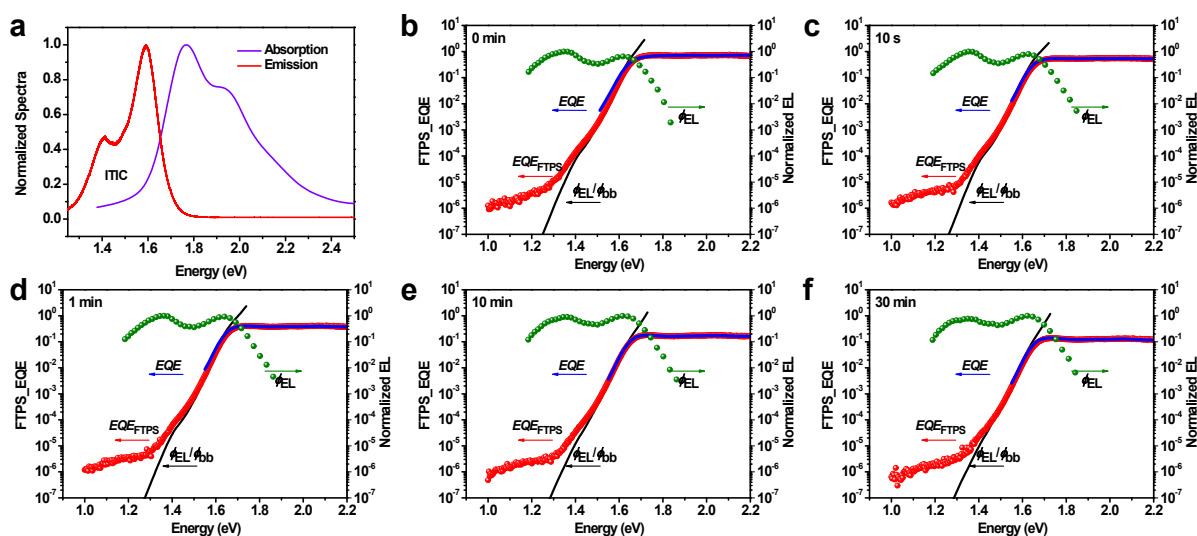


Figure S16. (a) Normalized absorption spectra and emission of pristine ITIC. Normalized FTSP-EQE, EQE, and EL of the J71:ITIC devices based on various exposure time periods including (b) 0 min, (c) 10 s, (d) 1 min, (e) 10 min and (f) 30 min, respectively.

Table S4. Summary of parameters measured and calculated from FTSP-EQE and EL.

Time periods	E_{gap} [eV]	V_{oc} [V]	V_{oc_loss} [V]	E_{CT} [V]	$\Delta E_1 = E_{gap} - qE_{CT}$	V_{oc}^{rad} [V]	$\Delta E_2 =$	$\Delta E_3 =$
--------------	----------------	--------------	--------------------	--------------	----------------------------------	--------------------	----------------	----------------

					[eV]			$E_{CT} - q\Delta V_{oc}^{rad}$	$q\Delta V_{oc}^{non-rad}$
								[eV]	[eV]
0 min	1.65	0.936	0.714	1.34	0.31	1.301	0.039	0.365	
10 s	1.65	0.904	0.746	1.35	0.30	1.303	0.047	0.399	
1 min	1.65	0.878	0.772	1.35	0.30	1.303	0.047	0.425	
10 min	1.65	0.839	0.811	1.36	0.29	1.302	0.058	0.463	
30 min	1.65	0.813	0.837	1.36	0.29	1.300	0.060	0.487	

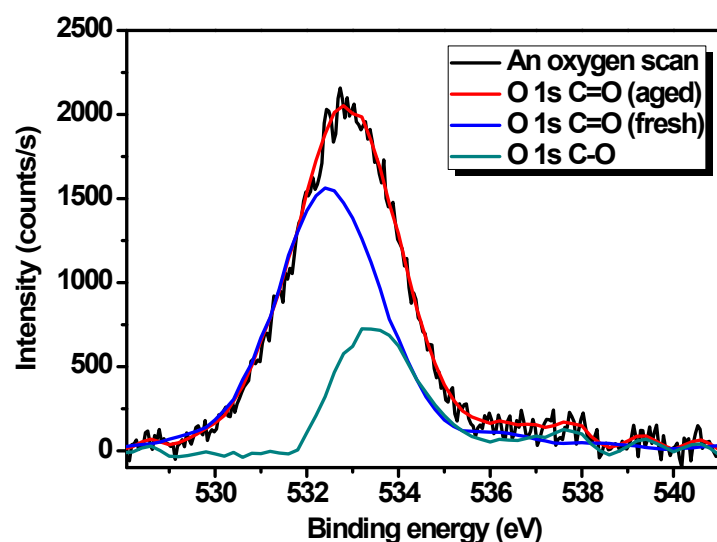


Figure S17. XPS O(1s) spectrum of J71:ITIC blends before and after 10 h exposure to light in air.

Table S5. The provenances of non-fullerene acceptors and fullerene derivatives.

Number	Material	Provenance	Ref	Number	Material	Provenance	Ref
1	ITIC	Solarmer Materials Inc	6	19	l-IDTBTRh	Erjun Zhou group	7
2	IT-M	Solarmer Materials Inc	8	20	IHIC	Solarmer Materials Inc	9
3	IT-DM	Solarmer Materials Inc	8	21	FOIC	Xiaowei Zhan group	10
4	ITCC	Solarmer Materials Inc	11	22	F8IC	Derthon Materials Inc	12
5	ITTC	Solarmer	13	23	C8IC	Derthon	14

		Materials Inc				Materials Inc	
6	ITCNTC	Chuluo Yang group	15	24	T8IC	Derthon Materials Inc	
7	MeIC	Chuluo Yang group	16	25	COi8DFIC	Liming Ding group	17
8	ITC-2Cl	Chuluo Yang group	5	26	Y5	Yingping Zou group	18
9	ITIC-Th	Solarmer Materials Inc	19	27	Y6	Derthon Materials Inc	20
10	IT-4F	Solarmer Materials Inc	21	28	INPIC-4F	Weihua Tang group	22
11	IT-4Cl	Solarmer Materials Inc	23	29	TPDI	Zhen Li group	24
12	NCBDT-4Cl	Solarmer Materials Inc	25	30	O-PYPDI	Zhen Li group	24
13	ITC6-IC	Weihua Tang group	26	31	O-PDI	Zhen Li group	24
14	IDIC	Solarmer Materials Inc	27	32	Th-PDI	Zhen Li group	24
15	O-IDTBR	Solarmer Materials Inc	28	33	TPYPDI	Zhen Li group	24
16	IDIC-4F	Solarmer Materials Inc	29	34	PCBM	Solarmer Materials Inc	
17	IDIC-4Cl	Solarmer Materials Inc	29	35	PC ₇₁ BM	Solarmer Materials Inc	
18	a-IDTBTRh	Erjun Zhou group	7				

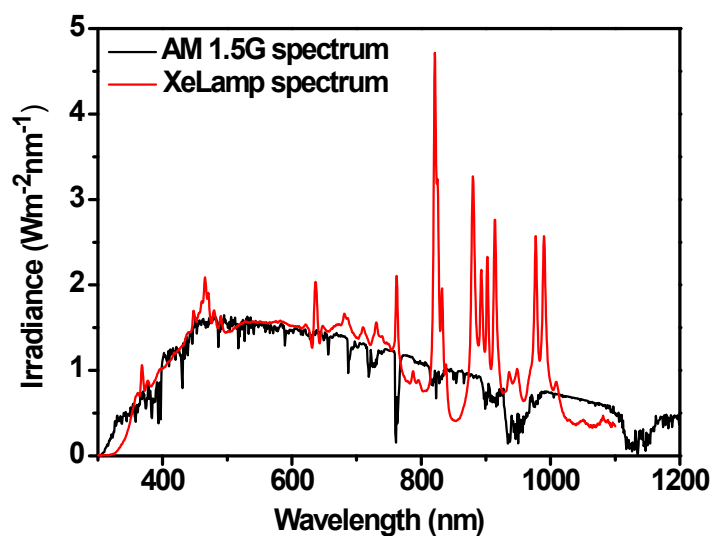


Figure S18. Emission spectrum of Xenon arc Lamp, and AM 1.5G spectrum of sun.

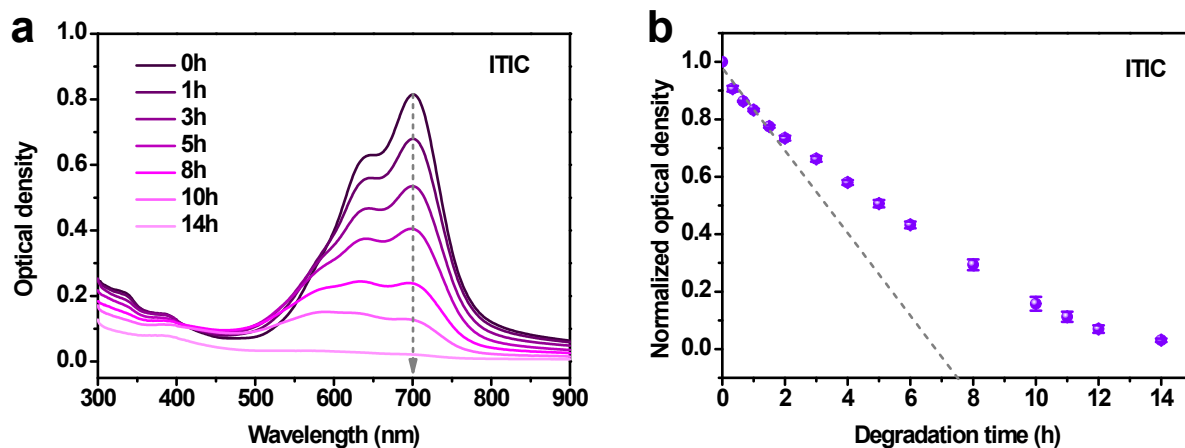


Figure S19. (a) Absorption spectra of ITIC film aged in ambient under 100 mW cm^{-2} illumination. (b) acceptor absorption peaks under illumination normalized by the initial maximum optical density before ageing. The error bars indicate the maximum and minimum values measured for the different equivalent samples. The dash lines indicate the fitted rates from the first few hours of ageing.

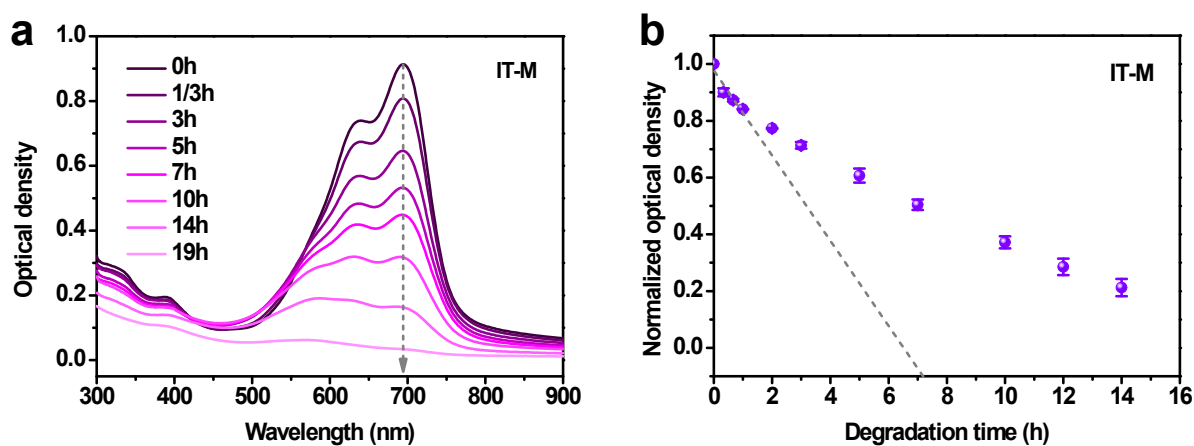


Figure S20. (a) Absorption spectra of IT-M film aged in ambient under 100 mW cm^{-2} illumination. (b) acceptor absorption peaks under illumination normalized by the initial maximum optical density before ageing. The error bars indicate the maximum and minimum values measured for the different equivalent samples. The dash lines indicate the fitted rates from the first few hours of ageing.

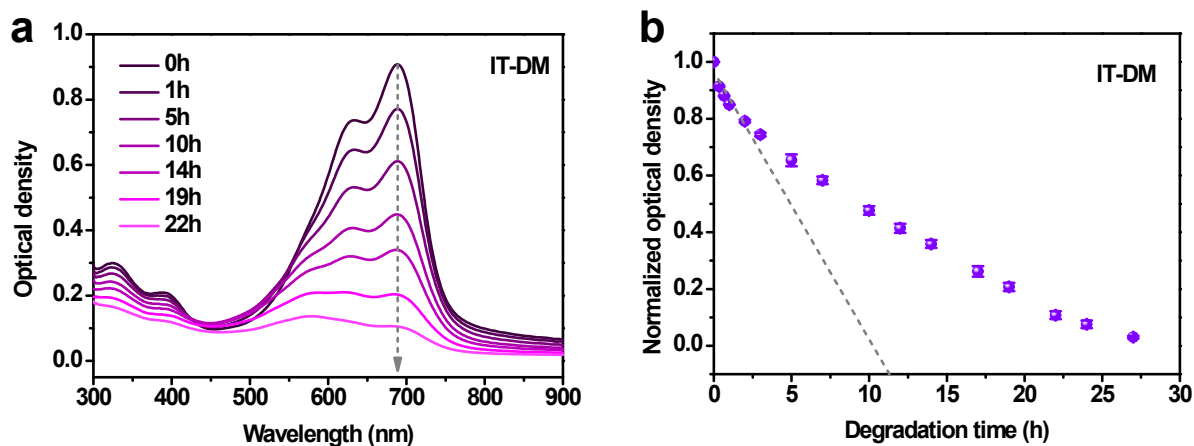


Figure S21. (a) Absorption spectra of IT-DM film aged in ambient under 100 mW cm^{-2} illumination. (b) acceptor absorption peaks under illumination normalized by the initial maximum optical density before ageing. The error bars indicate the maximum and minimum values measured for the different equivalent samples. The dash lines indicate the fitted rates from the first few hours of ageing.

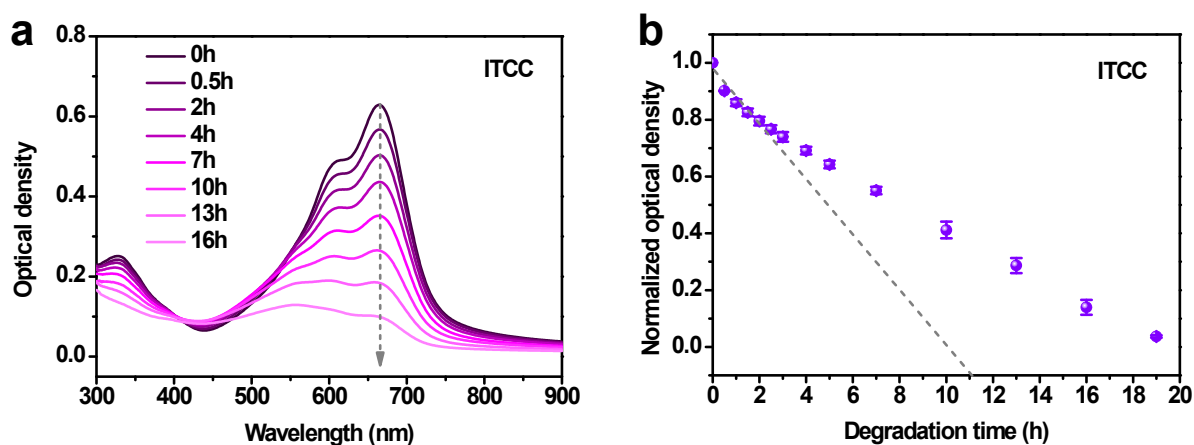


Figure S22. (a) Absorption spectra of ITCC film aged in ambient under 100 mW cm^{-2} illumination. (b) acceptor absorption peaks under illumination normalized by the initial maximum optical density before ageing. The error bars indicate the maximum and minimum values measured for the different equivalent samples. The dash lines indicate the fitted rates from the first few hours of ageing.

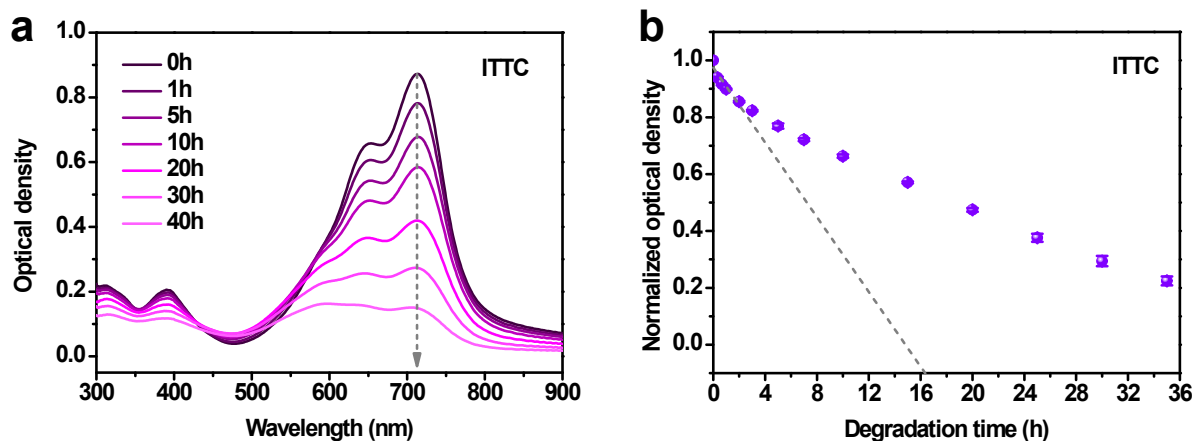


Figure S23. (a) Absorption spectra of ITTC film aged in ambient under 100 mW cm^{-2} illumination. (b) acceptor absorption peaks under illumination normalized by the initial maximum optical density before ageing. The error bars indicate the maximum and minimum values measured for the different equivalent samples. The dash lines indicate the fitted rates from the first few hours of ageing.

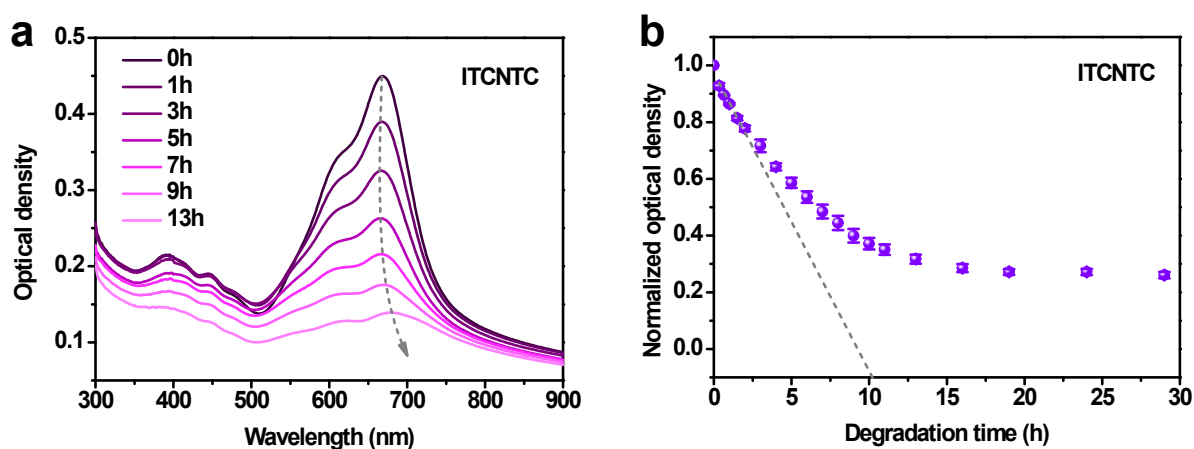


Figure S24. (a) Absorption spectra of ITCNTC film aged in ambient under 100 mW cm^{-2} illumination. (b) acceptor absorption peaks under illumination normalized by the initial maximum optical density before ageing. The error bars indicate the maximum and minimum values measured for the different equivalent samples. The dash lines indicate the fitted rates from the first few hours of ageing.

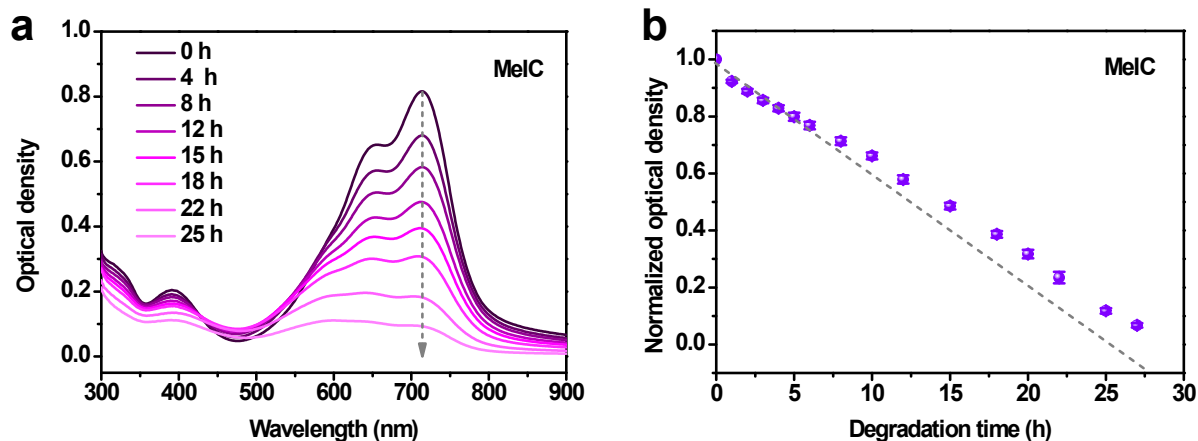


Figure S25. (a) Absorption spectra of MeIC film aged in ambient under 100 mW cm^{-2} illumination. (b) acceptor absorption peaks under illumination normalized by the initial maximum optical density before ageing. The error bars indicate the maximum and minimum values measured for the different equivalent samples. The dash lines indicate the fitted rates from the first few hours of ageing.

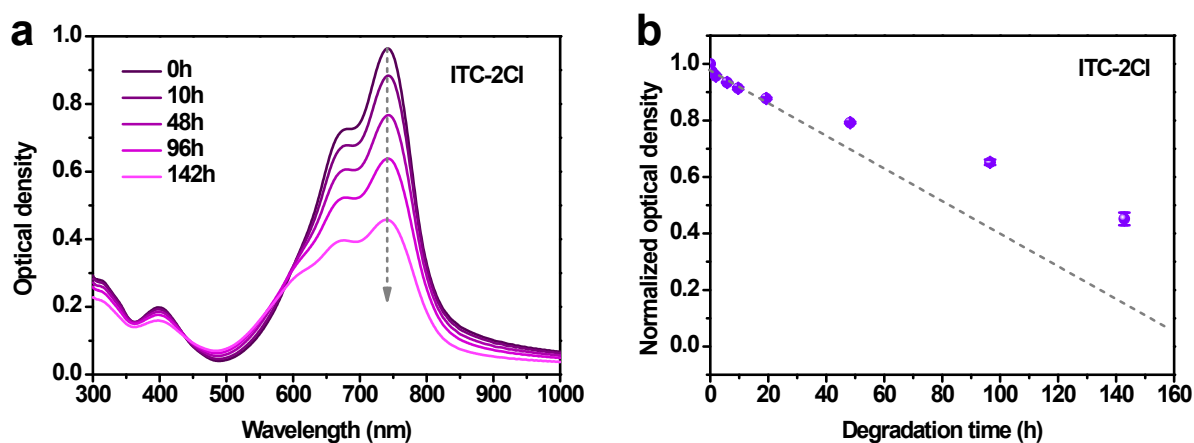


Figure S26. (a) Absorption spectra of ITC-2Cl film aged in ambient under 100 mW cm^{-2} illumination. (b) acceptor absorption peaks under illumination normalized by the initial maximum optical density before ageing. The error bars indicate the maximum and minimum values measured for the different equivalent samples. The dash lines indicate the fitted rates from the first few hours of ageing.

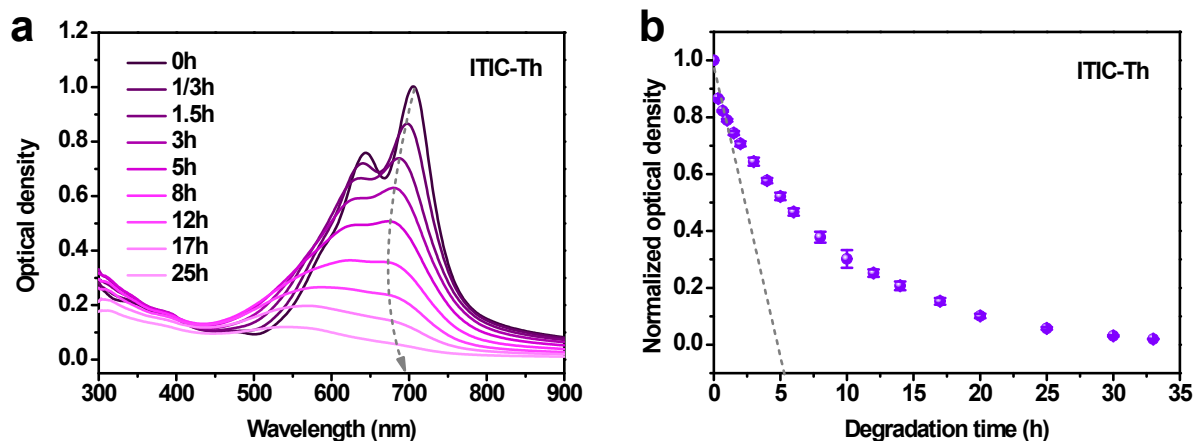


Figure S27. (a) Absorption spectra of ITIC-Th film aged in ambient under 100 mW cm^{-2} illumination. (b) acceptor absorption peaks under illumination normalized by the initial maximum optical density before ageing. The error bars indicate the maximum and minimum values measured for the different equivalent samples. The dash lines indicate the fitted rates from the first few hours of ageing.

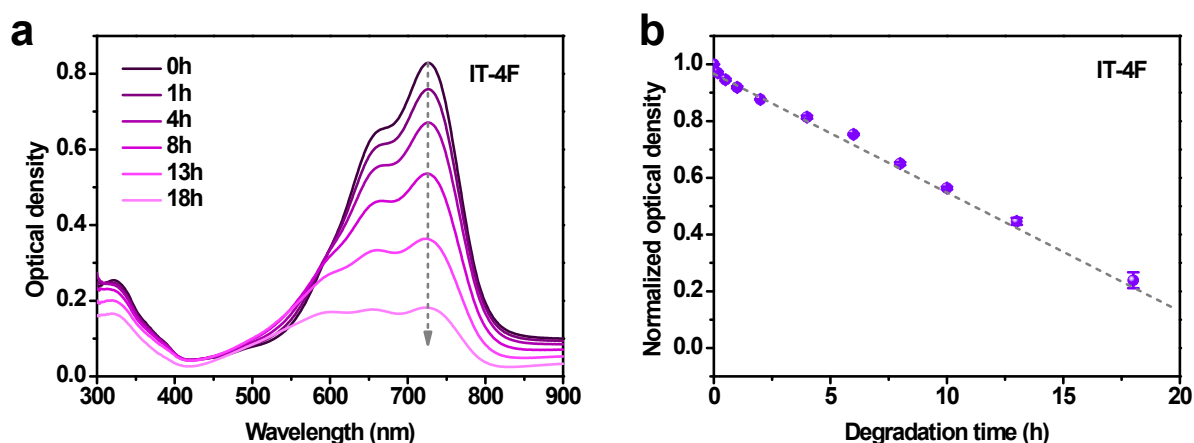


Figure S28. (a) Absorption spectra of IT-4F film aged in ambient under 100 mW cm^{-2} illumination. (b) acceptor absorption peaks under illumination normalized by the initial maximum optical density before ageing. The error bars indicate the maximum and minimum values measured for the different equivalent samples. The dash lines indicate the fitted rates from the first few hours of ageing.

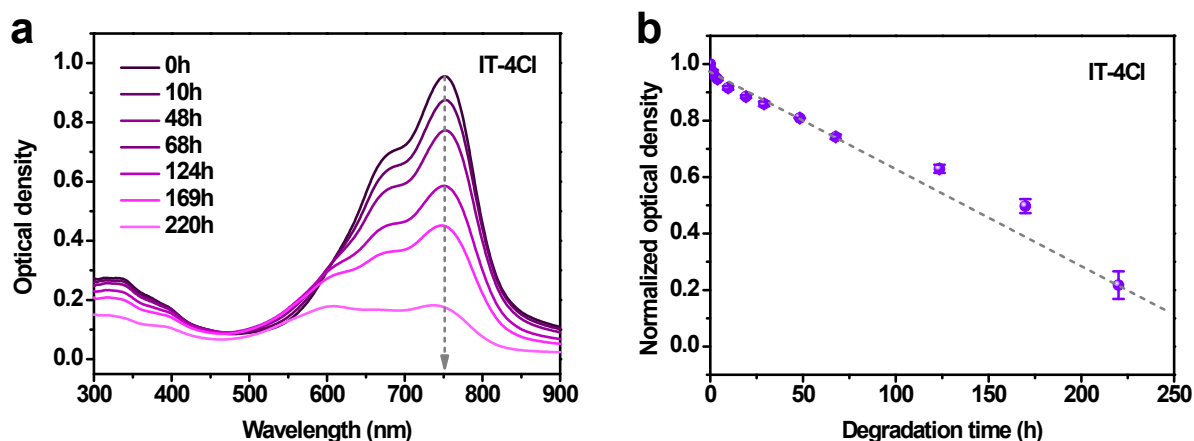


Figure S29. (a) Absorption spectra of IT-4Cl film aged in ambient under 100 mW cm^{-2} illumination. (b) acceptor absorption peaks under illumination normalized by the initial maximum optical density before ageing. The error bars indicate the maximum and minimum values measured for the different equivalent samples. The dash lines indicate the fitted rates from the first few hours of ageing.

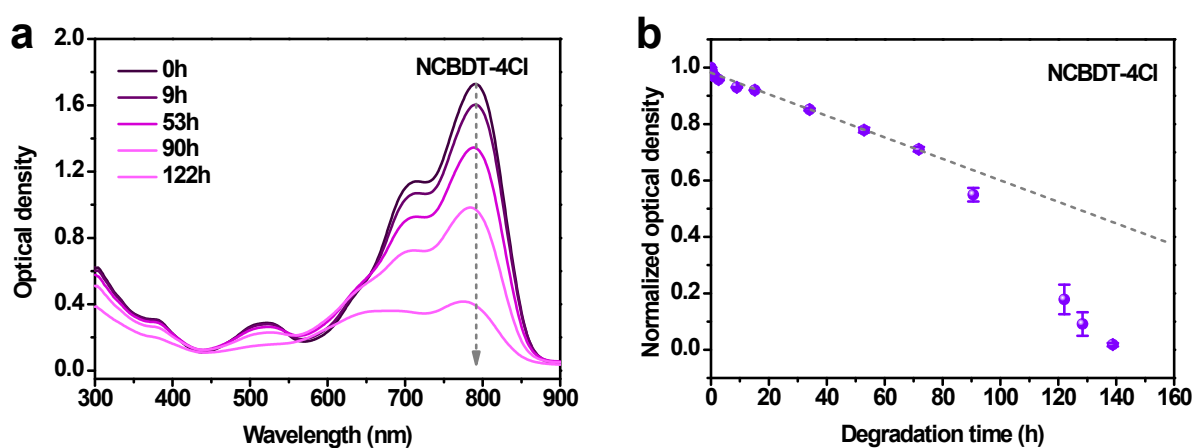


Figure S30. (a) Absorption spectra of NCBDT-4Cl film aged in ambient under 100 mW cm^{-2} illumination. (b) acceptor absorption peaks under illumination normalized by the initial maximum optical density before ageing. The error bars indicate the maximum and minimum values measured for the different equivalent samples. The dash lines indicate the fitted rates from the first few hours of ageing.

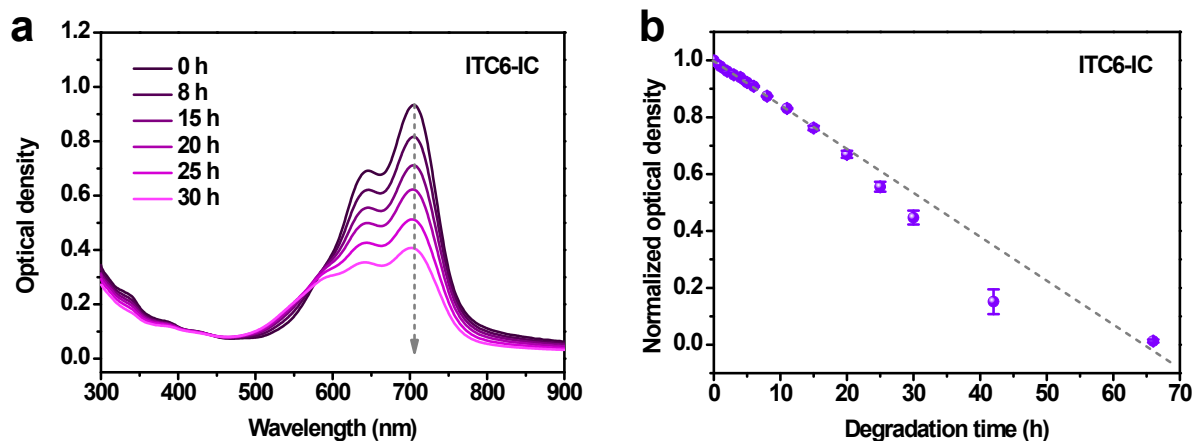


Figure S31. (a) Absorption spectra of ITC6-IC film aged in ambient under 100 mW cm^{-2} illumination. (b) acceptor absorption peaks under illumination normalized by the initial maximum optical density before ageing. The error bars indicate the maximum and minimum values measured for the different equivalent samples. The dash lines indicate the fitted rates from the first few hours of ageing.

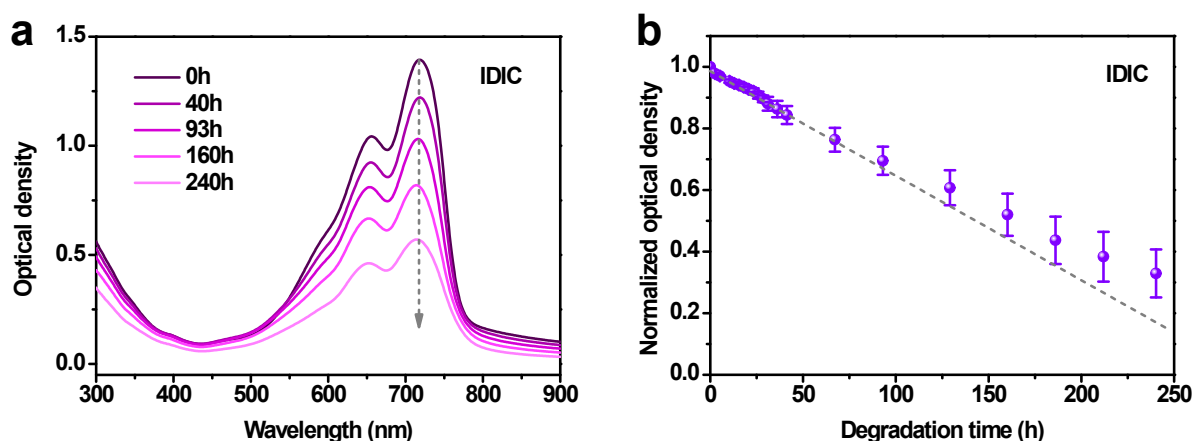


Figure S32. (a) Absorption spectra of IDIC film aged in ambient under 100 mW cm^{-2} illumination. (b) acceptor absorption peaks under illumination normalized by the initial maximum optical density before ageing. The error bars indicate the maximum and minimum values measured for the different equivalent samples. The dash lines indicate the fitted rates from the first few hours of ageing.

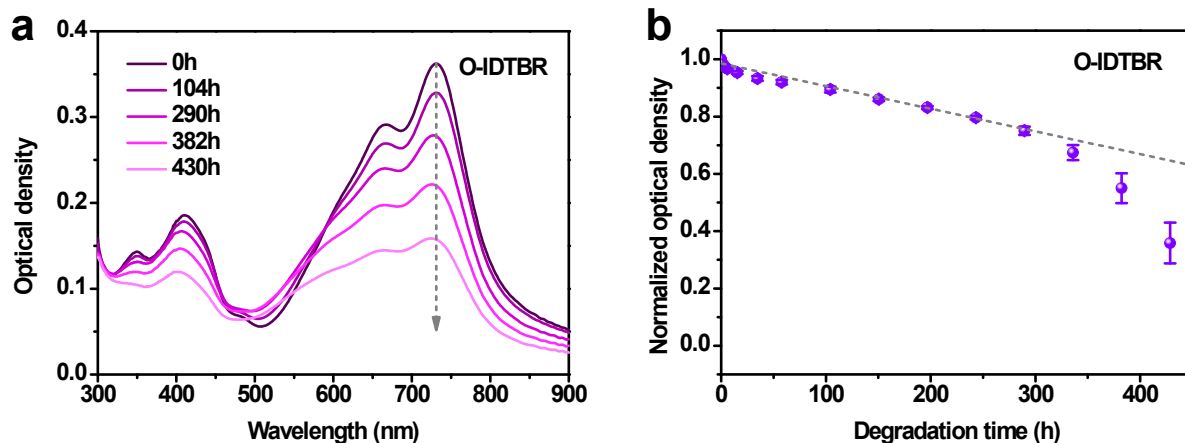


Figure S33. (a) Absorption spectra of O-IDTBR film aged in ambient under 100 mW cm^{-2} illumination. (b) acceptor absorption peaks under illumination normalized by the initial maximum optical density before ageing. The error bars indicate the maximum and minimum values measured for the different equivalent samples. The dash lines indicate the fitted rates from the first few hours of ageing.

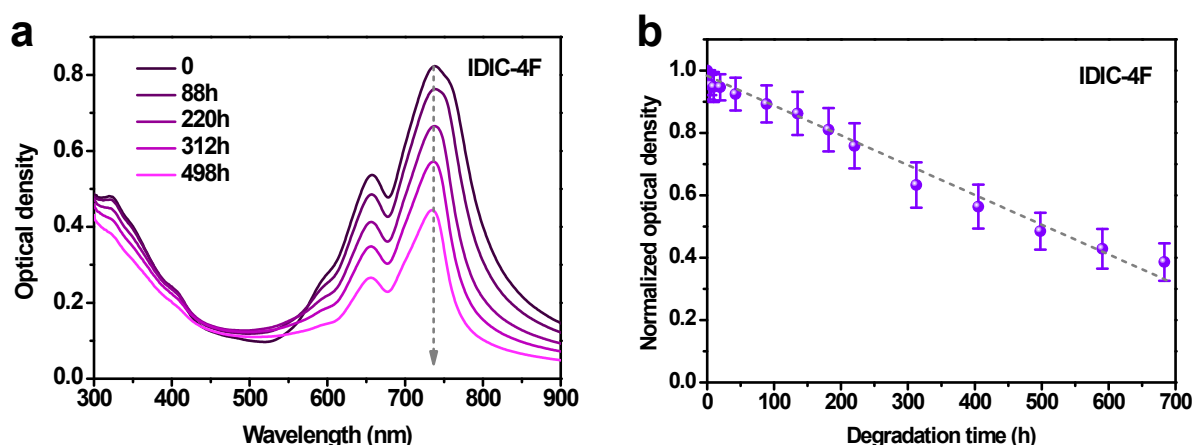


Figure S34. (a) Absorption spectra of IDIC-4F film aged in ambient under 100 mW cm^{-2} illumination. (b) acceptor absorption peaks under illumination normalized by the initial maximum optical density before ageing. The error bars indicate the maximum and minimum values measured for the different equivalent samples. The dash lines indicate the fitted rates from the first few hours of ageing.

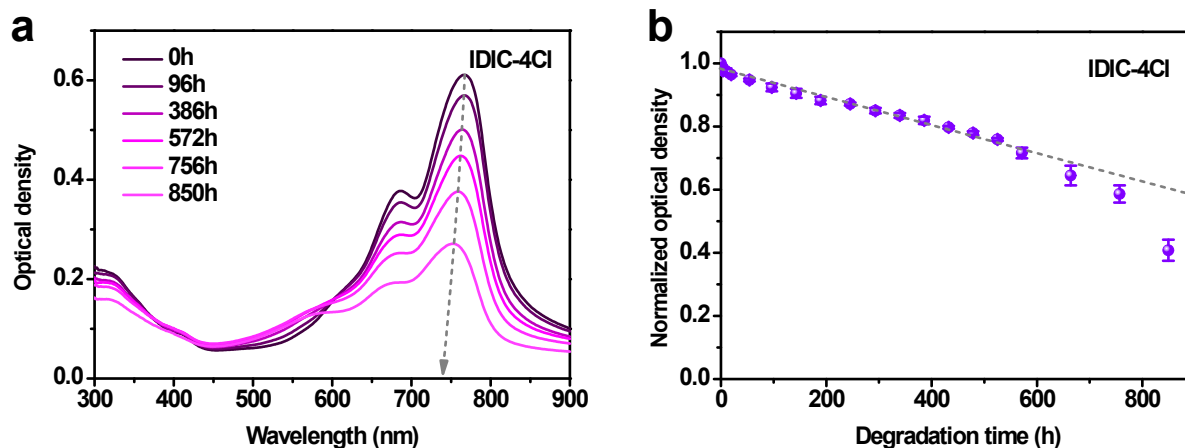


Figure S35. (a) Absorption spectra of IDIC-4Cl film aged in ambient under 100 mW cm^{-2} illumination. (b) acceptor absorption peaks under illumination normalized by the initial maximum optical density before ageing. The error bars indicate the maximum and minimum values measured for the different equivalent samples. The dash lines indicate the fitted rates from the first few hours of ageing.

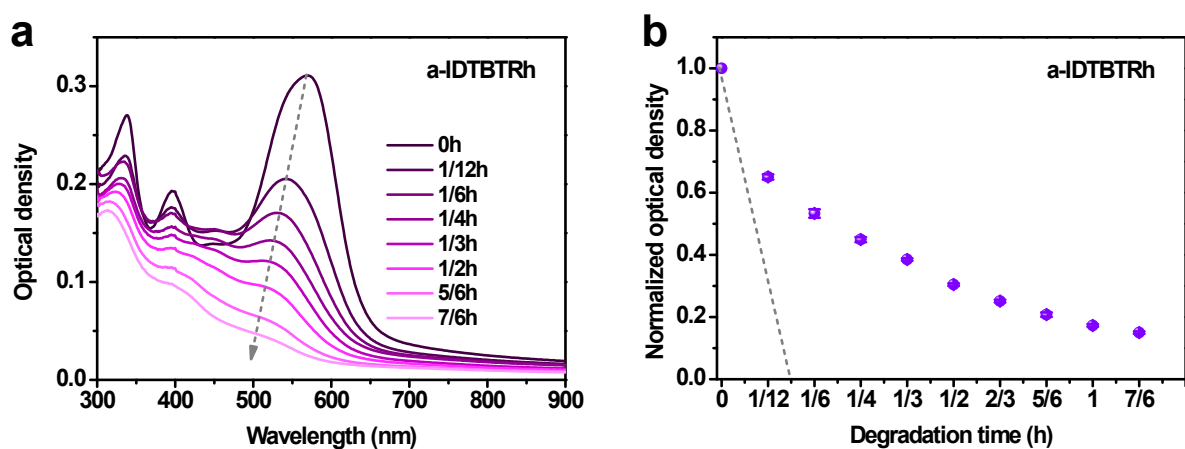


Figure S36. (a) Absorption spectra of a-IDTBTRh film aged in ambient under 100 mW cm^{-2} illumination. (b) acceptor absorption peaks under illumination normalized by the initial maximum optical density before ageing. The error bars indicate the maximum and minimum values measured for the different equivalent samples. The dash lines indicate the fitted rates from the first few hours of ageing.

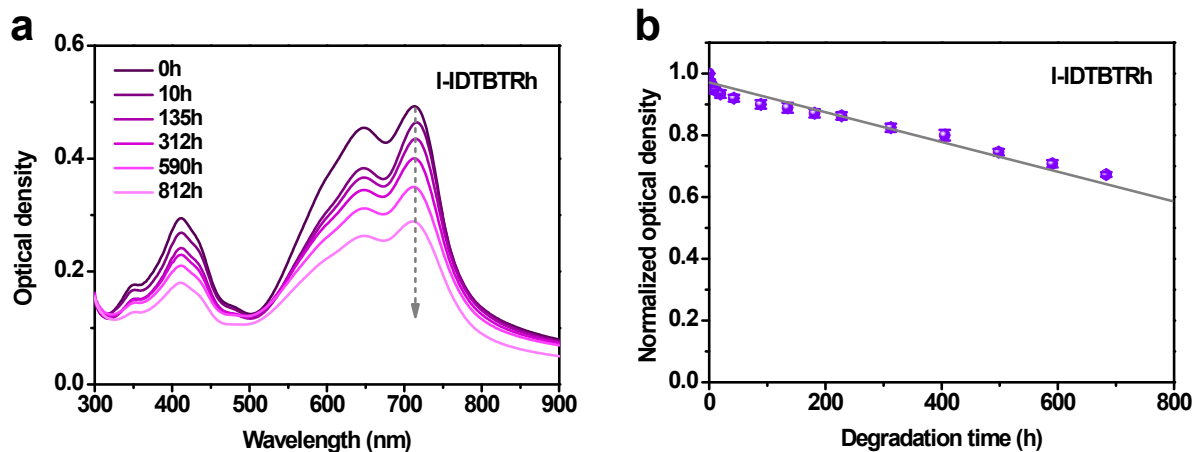


Figure S37. (a) Absorption spectra of l-IDTBTRh film aged in ambient under 100 mW cm^{-2} illumination. (b) acceptor absorption peaks under illumination normalized by the initial maximum optical density before ageing. The error bars indicate the maximum and minimum values measured for the different equivalent samples. The dash lines indicate the fitted rates from the first few hours of ageing.

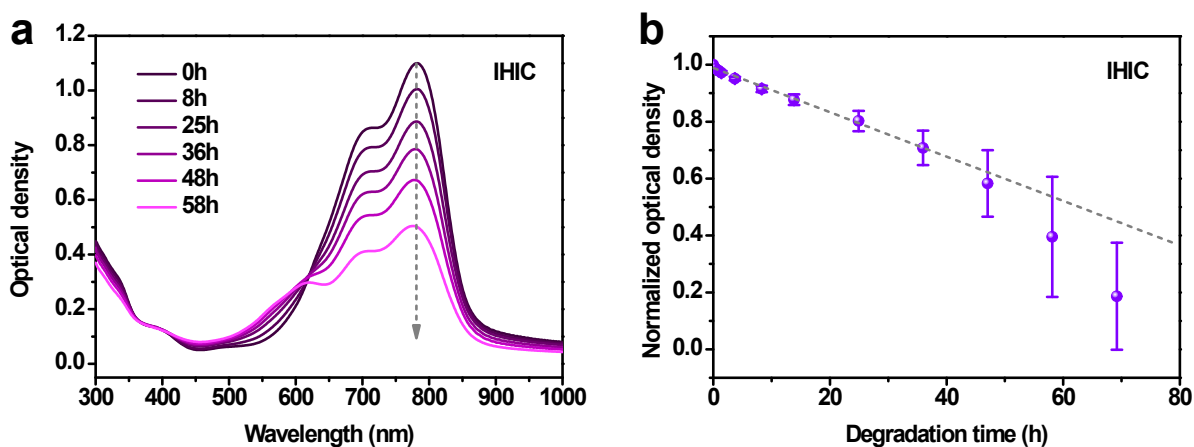


Figure S38. (a) Absorption spectra of IHIC film aged in ambient under 100 mW cm^{-2} illumination. (b) acceptor absorption peaks under illumination normalized by the initial maximum optical density before ageing. The error bars indicate the maximum and minimum values measured for the different equivalent samples. The dash lines indicate the fitted rates from the first few hours of ageing.

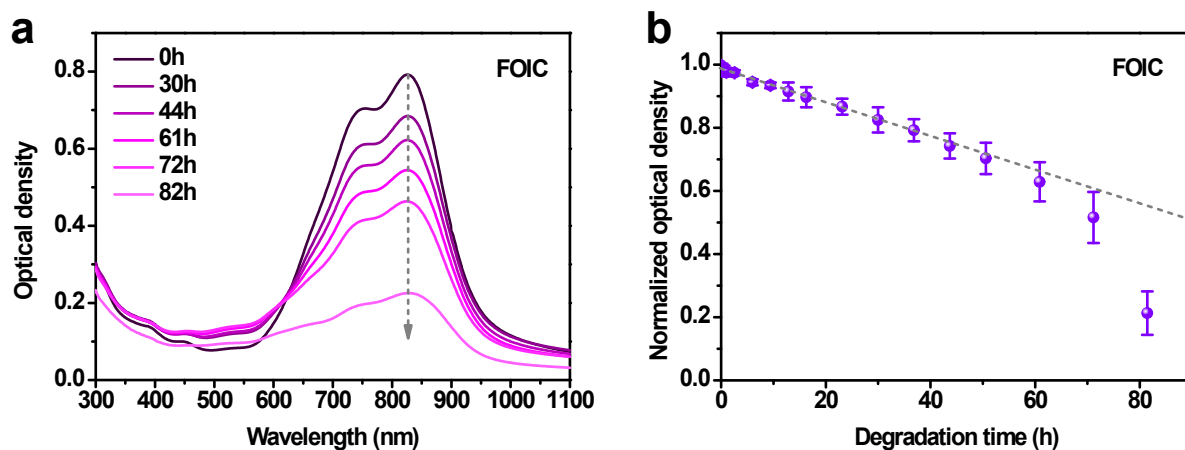


Figure S39. (a) Absorption spectra of FOIC film aged in ambient under 100 mW cm^{-2} illumination. (b) acceptor absorption peaks under illumination normalized by the initial maximum optical density before ageing. The error bars indicate the maximum and minimum values measured for the different equivalent samples. The dash lines indicate the fitted rates from the first few hours of ageing.

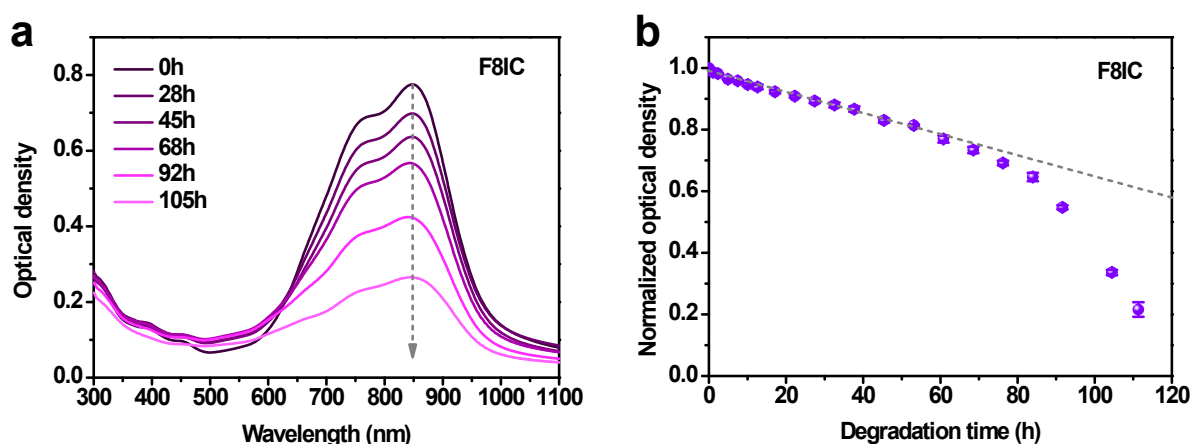


Figure S40. (a) Absorption spectra of F8IC film aged in ambient under 100 mW cm^{-2} illumination. (b) acceptor absorption peaks under illumination normalized by the initial maximum optical density before ageing. The error bars indicate the maximum and minimum values measured for the different equivalent samples. The dash lines indicate the fitted rates from the first few hours of ageing.

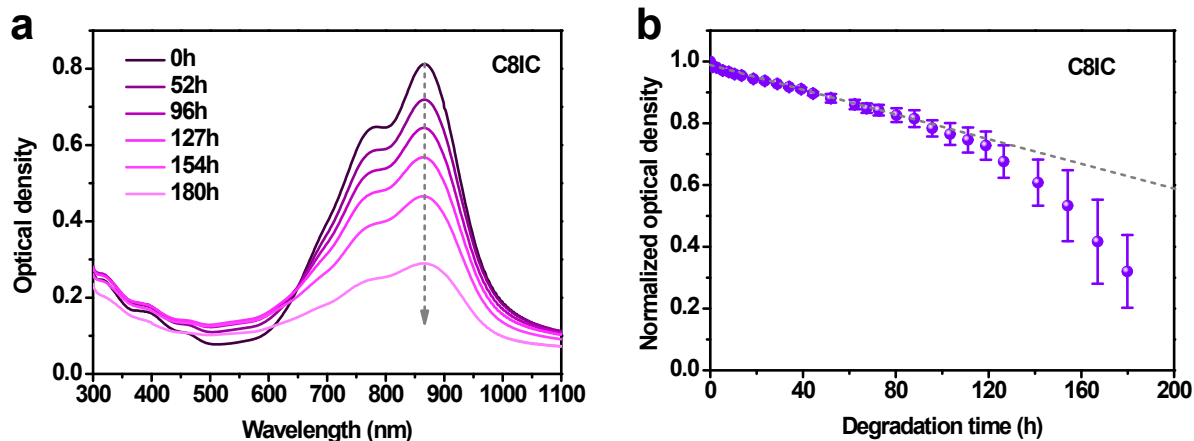


Figure S41. (a) Absorption spectra of C8IC film aged in ambient under 100 mW cm^{-2} illumination. (b) acceptor absorption peaks under illumination normalized by the initial maximum optical density before ageing. The error bars indicate the maximum and minimum values measured for the different equivalent samples. The dash lines indicate the fitted rates from the first few hours of ageing.

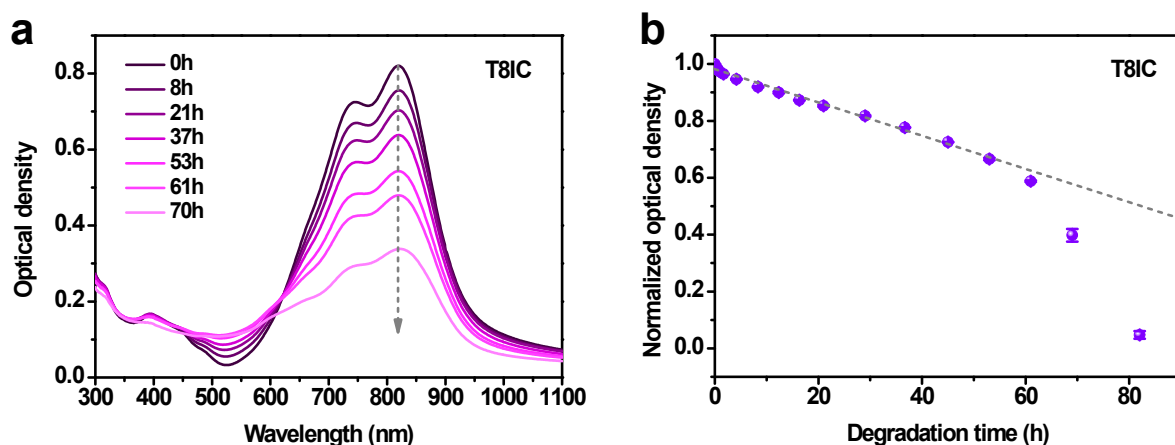


Figure S42. (a) Absorption spectra of T8IC film aged in ambient under 100 mW cm^{-2} illumination. (b) acceptor absorption peaks under illumination normalized by the initial maximum optical density before ageing. The error bars indicate the maximum and minimum values measured for the different equivalent samples. The dash lines indicate the fitted rates from the first few hours of ageing.

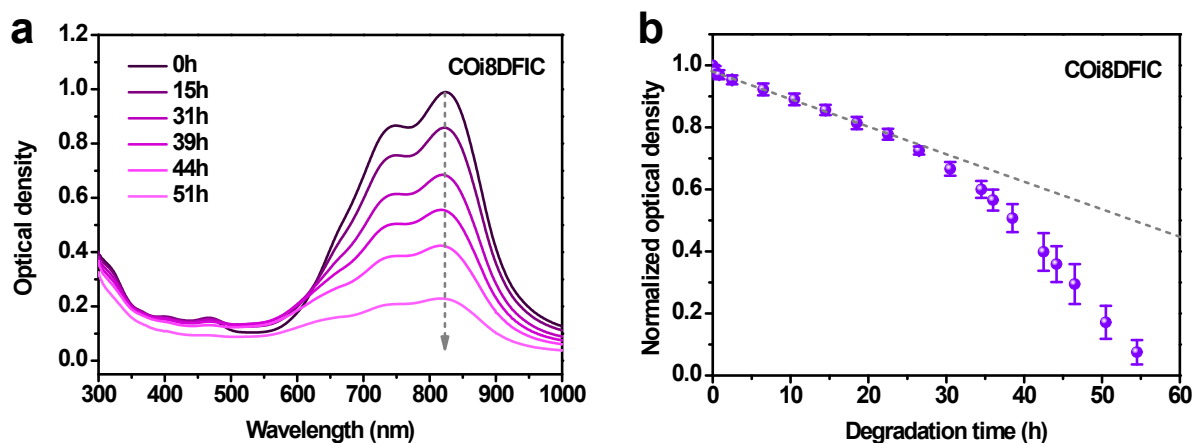


Figure S43. (a) Absorption spectra of COi8DFIC film aged in ambient under 100 mW cm^{-2} illumination. (b) acceptor absorption peaks under illumination normalized by the initial maximum optical density before ageing. The error bars indicate the maximum and minimum values measured for the different equivalent samples. The dash lines indicate the fitted rates from the first few hours of ageing.

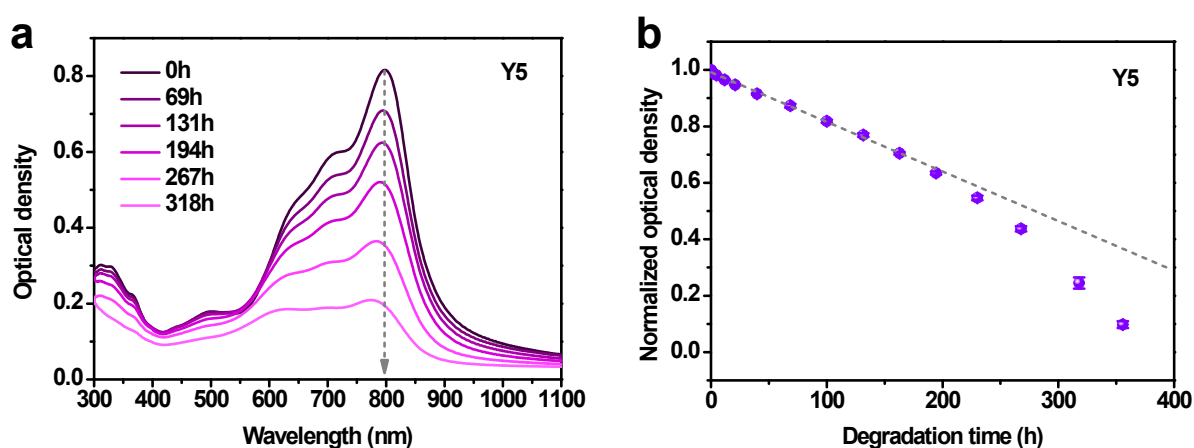


Figure S44. (a) Absorption spectra of Y5 film aged in ambient under 100 mW cm^{-2} illumination. (b) acceptor absorption peaks under illumination normalized by the initial maximum optical density before ageing. The error bars indicate the maximum and minimum values measured for the different equivalent samples. The dash lines indicate the fitted rates from the first few hours of ageing.

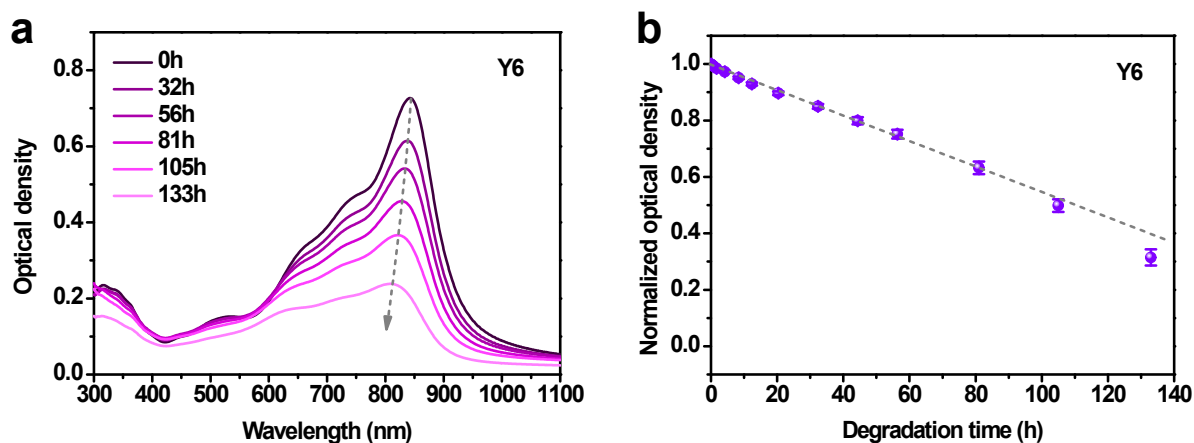


Figure S45. (a) Absorption spectra of Y6 film aged in ambient under 100 mW cm^{-2} illumination. (b) acceptor absorption peaks under illumination normalized by the initial maximum optical density before ageing. The error bars indicate the maximum and minimum values measured for the different equivalent samples. The dash lines indicate the fitted rates from the first few hours of ageing.

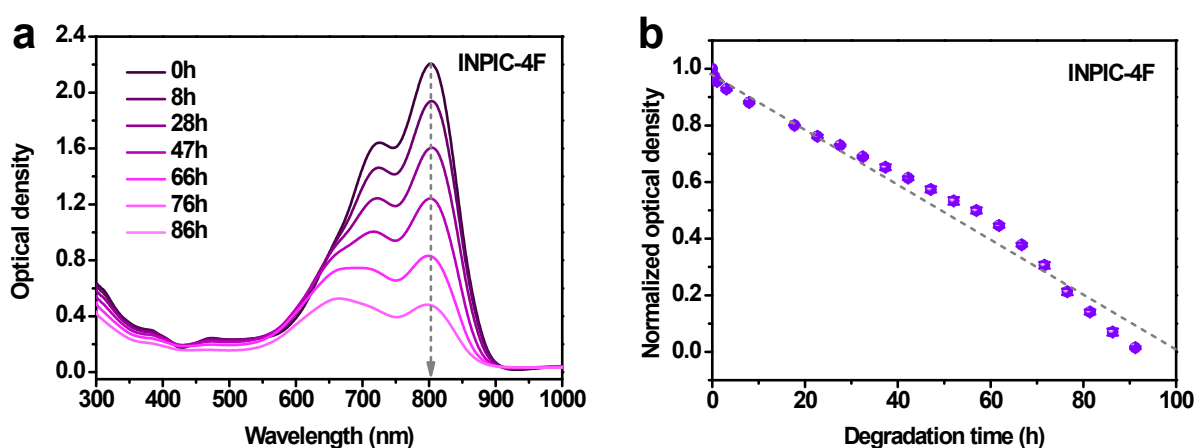


Figure S46. (a) Absorption spectra of INPIC-4F film aged in ambient under 100 mW cm^{-2} illumination. (b) acceptor absorption peaks under illumination normalized by the initial maximum optical density before ageing. The error bars indicate the maximum and minimum values measured for the different equivalent samples. The dash lines indicate the fitted rates from the first few hours of ageing.

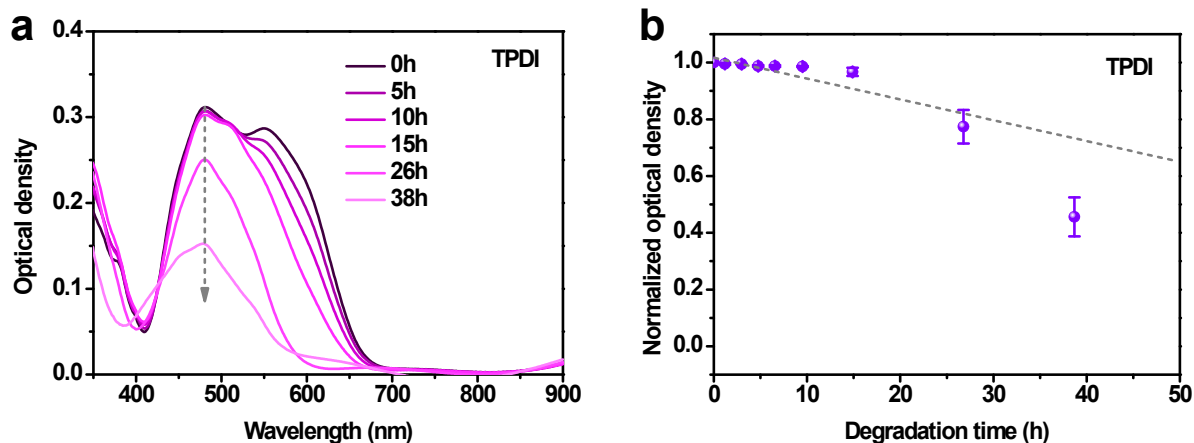


Figure S47. (a) Absorption spectra of TPDI film aged in ambient under 100 mW cm^{-2} illumination. (b) acceptor absorption peaks under illumination normalized by the initial maximum optical density before ageing. The error bars indicate the maximum and minimum values measured for the different equivalent samples. The dash lines indicate the fitted rates from the first few hours of ageing.

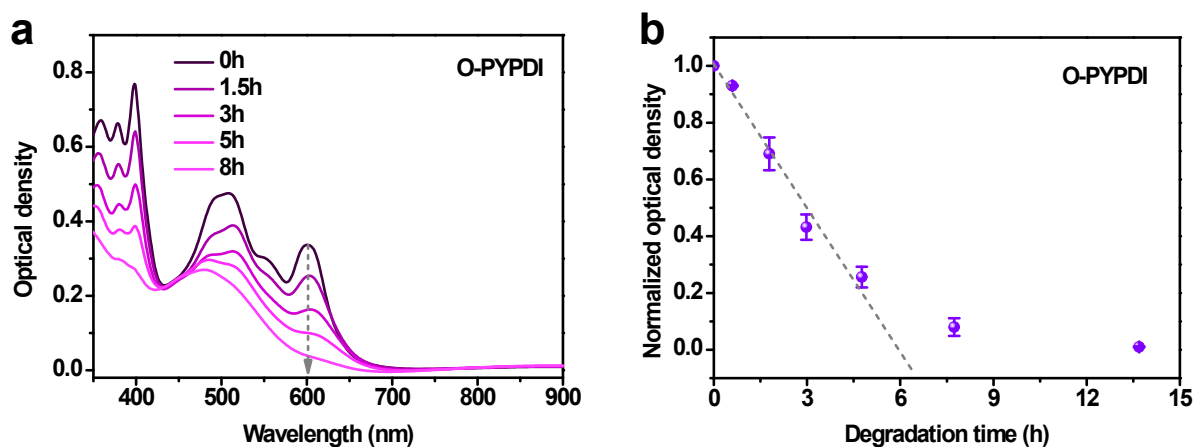


Figure S48. (a) Absorption spectra of O-PYPDI film aged in ambient under 100 mW cm^{-2} illumination. (b) acceptor absorption peaks under illumination normalized by the initial maximum optical density before ageing. The error bars indicate the maximum and minimum values measured for the different equivalent samples. The dash lines indicate the fitted rates from the first few hours of ageing.

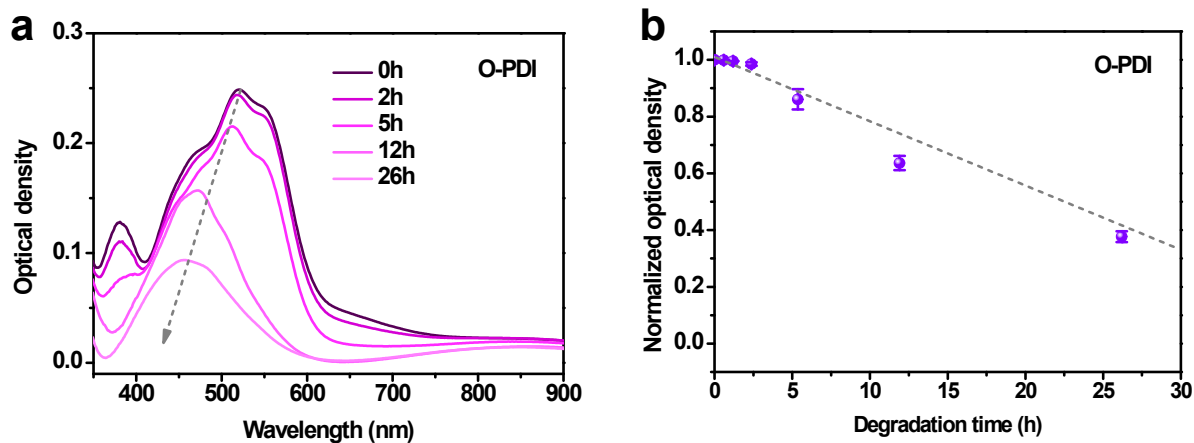


Figure S49. (a) Absorption spectra of O-PDI film aged in ambient under 100 mW cm^{-2} illumination. (b) acceptor absorption peaks under illumination normalized by the initial maximum optical density before ageing. The error bars indicate the maximum and minimum values measured for the different equivalent samples. The dash lines indicate the fitted rates from the first few hours of ageing.

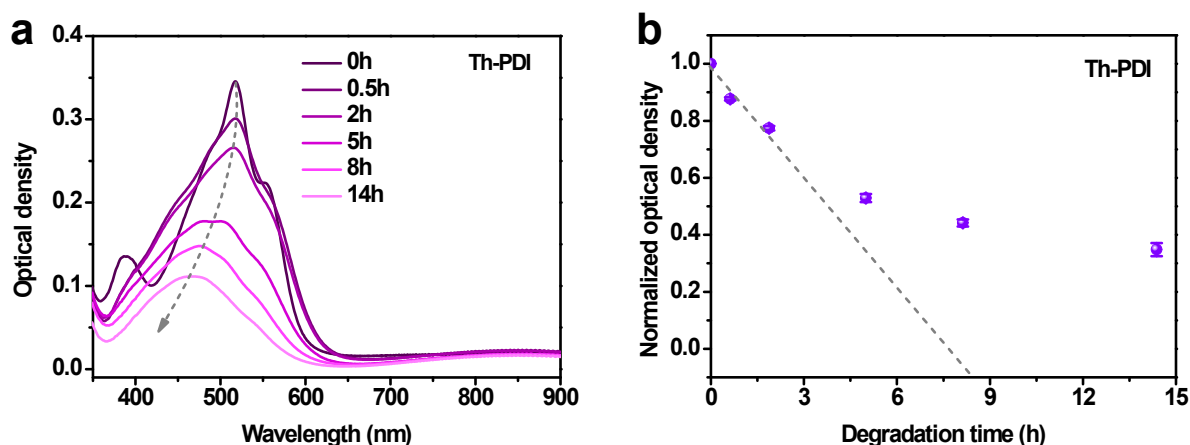


Figure S50. (a) Absorption spectra of Th-PDI film aged in ambient under 100 mW cm^{-2} illumination. (b) acceptor absorption peaks under illumination normalized by the initial maximum optical density before ageing. The error bars indicate the maximum and minimum values measured for the different equivalent samples. The dash lines indicate the fitted rates from the first few hours of ageing.

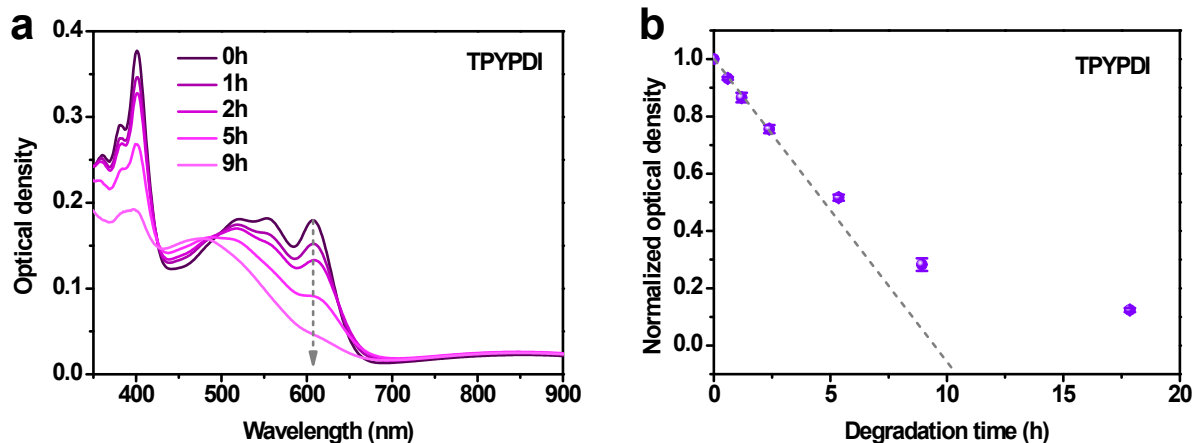


Figure S51. (a) Absorption spectra of TPYPDI film aged in ambient under 100 mW cm^{-2} illumination. (b) acceptor absorption peaks under illumination normalized by the initial maximum optical density before ageing. The error bars indicate the maximum and minimum values measured for the different equivalent samples. The dash lines indicate the fitted rates from the first few hours of ageing.

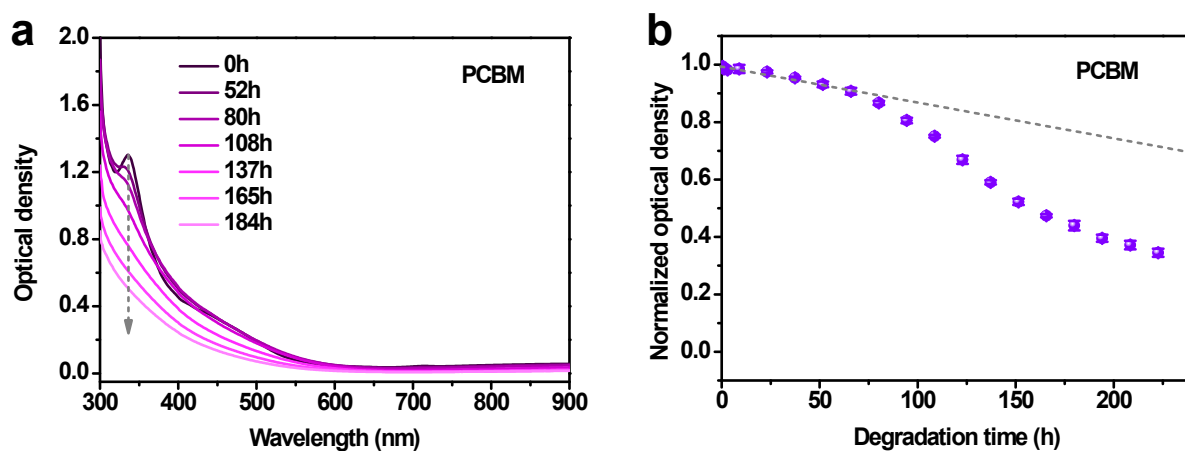


Figure S52. (a) Absorption spectra of PCBM film aged in ambient under 100 mW cm^{-2} illumination. (b) acceptor absorption peaks under illumination normalized by the initial maximum optical density before ageing. The error bars indicate the maximum and minimum values measured for the different equivalent samples. The dash lines indicate the fitted rates from the first few hours of ageing.

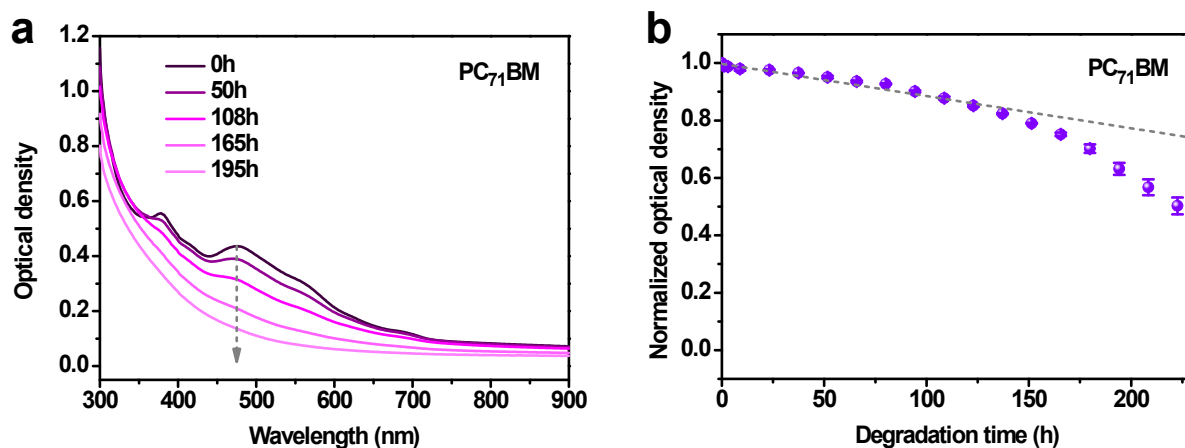


Figure S53. (a) Absorption spectra of PC₇₁BM film aged in ambient under 100 mW cm⁻² illumination. (b) acceptor absorption peaks under illumination normalized by the initial maximum optical density before ageing. The error bars indicate the maximum and minimum values measured for the different equivalent samples. The dash lines indicate the fitted rates from the first few hours of ageing.

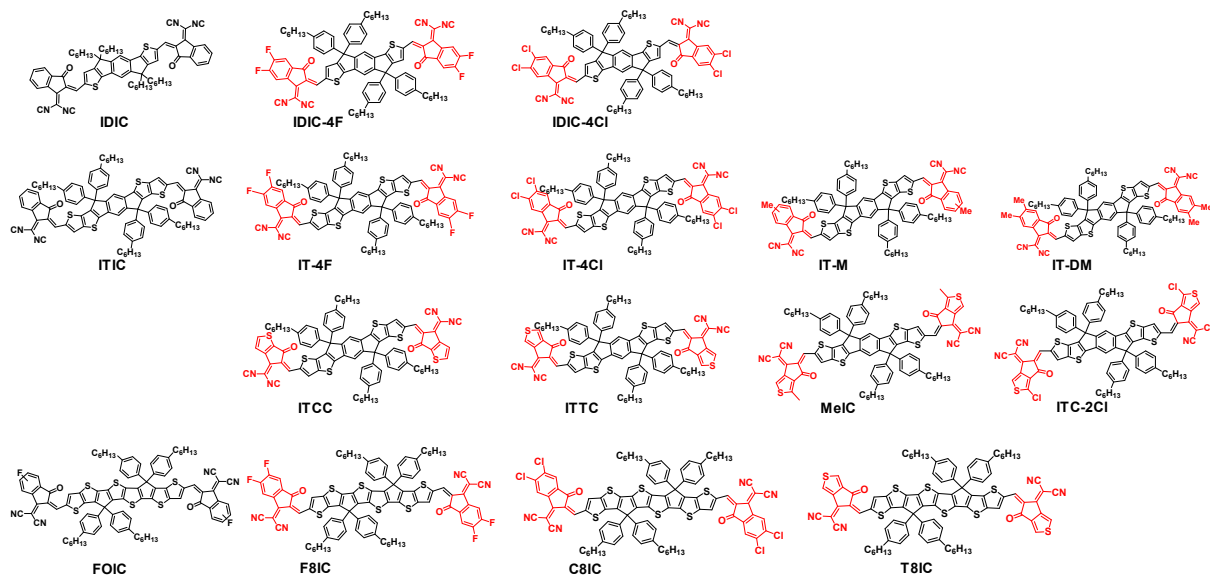


Figure S54. Molecule structures of IDIC, ITIC, and FOIC as well as their derivatives.

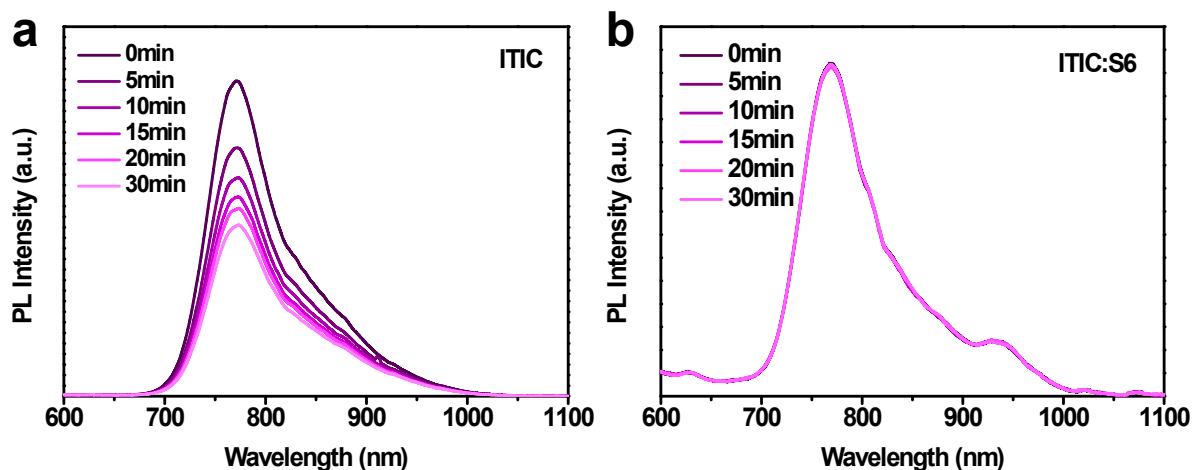


Figure S55. PL spectra of ITIC films without and with 2 wt% S6 aged under continuous 405nm laser light irradiation.

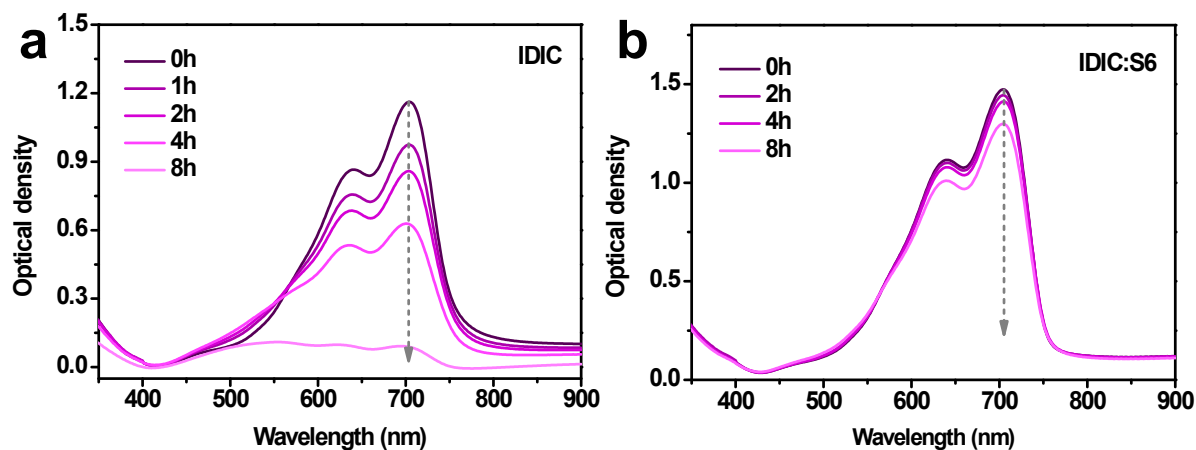


Figure S56. Absorption spectra of IDIC films without and with 2 wt% S6 aged in ambient under 100 mW cm^{-2} illumination.

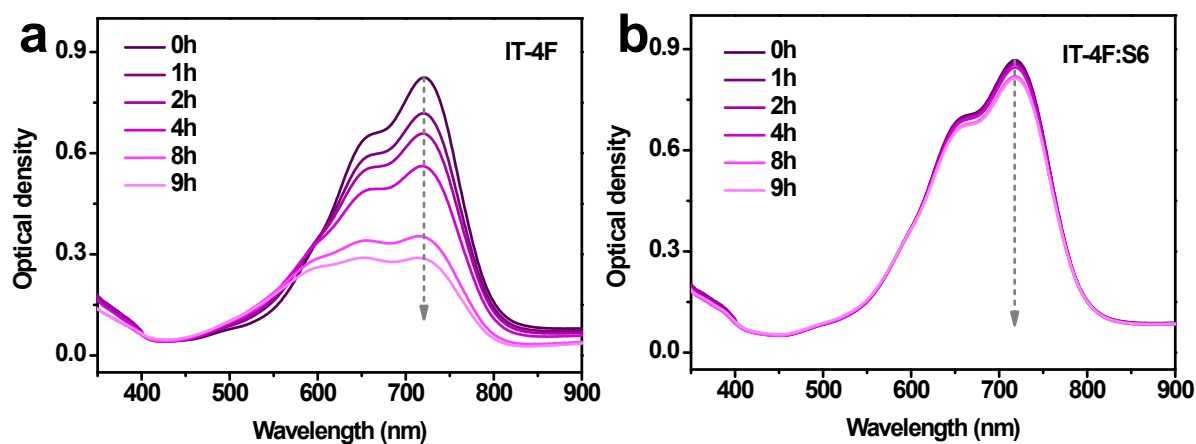


Figure S57. Absorption spectra of IT-4F films without and with 2 wt% S6 aged in ambient under 100 mW cm^{-2} illumination.

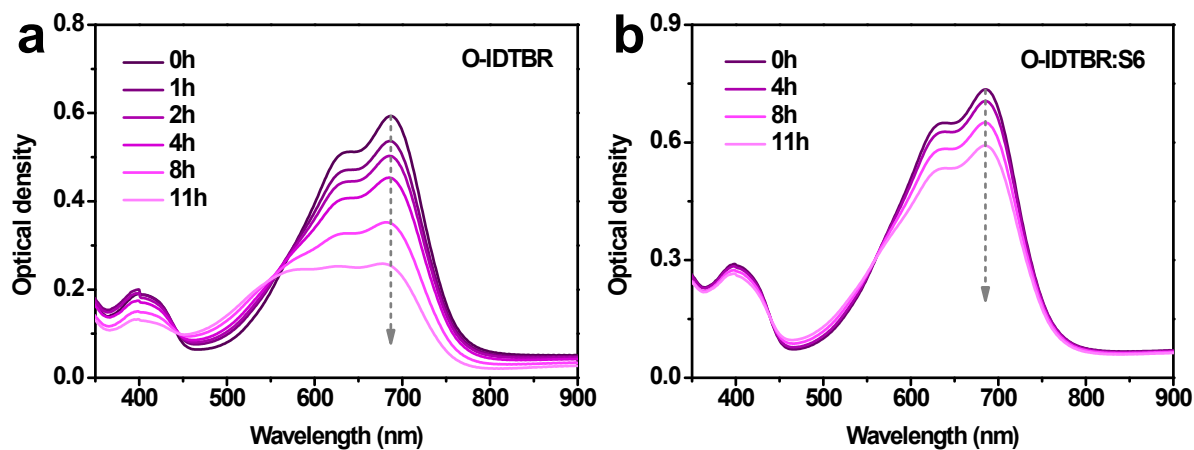


Figure S58. Absorption spectra of O-IDTBR films without and with 2 wt% S6 aged in ambient under 100 mW cm^{-2} illumination.

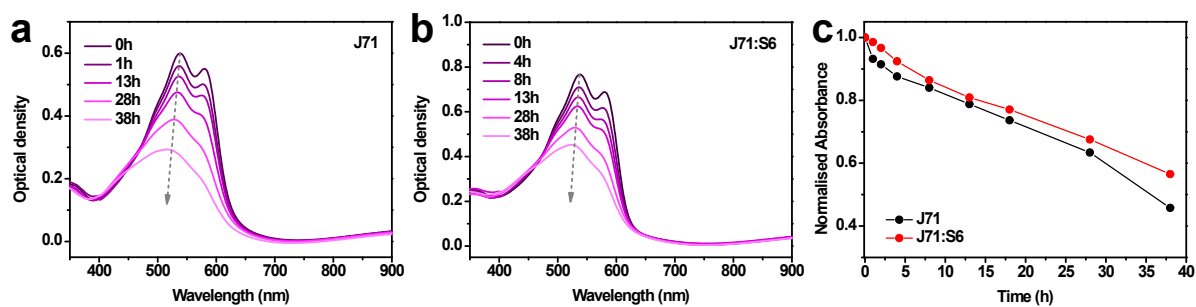


Figure S59. Absorption spectra of polymer J71 (a) without and (b) with 2 wt% S6 aged in ambient under 100 mW cm^{-2} illumination. (c) Degradation kinetics of J71 without (dark) and with (red) 2 wt% S6.

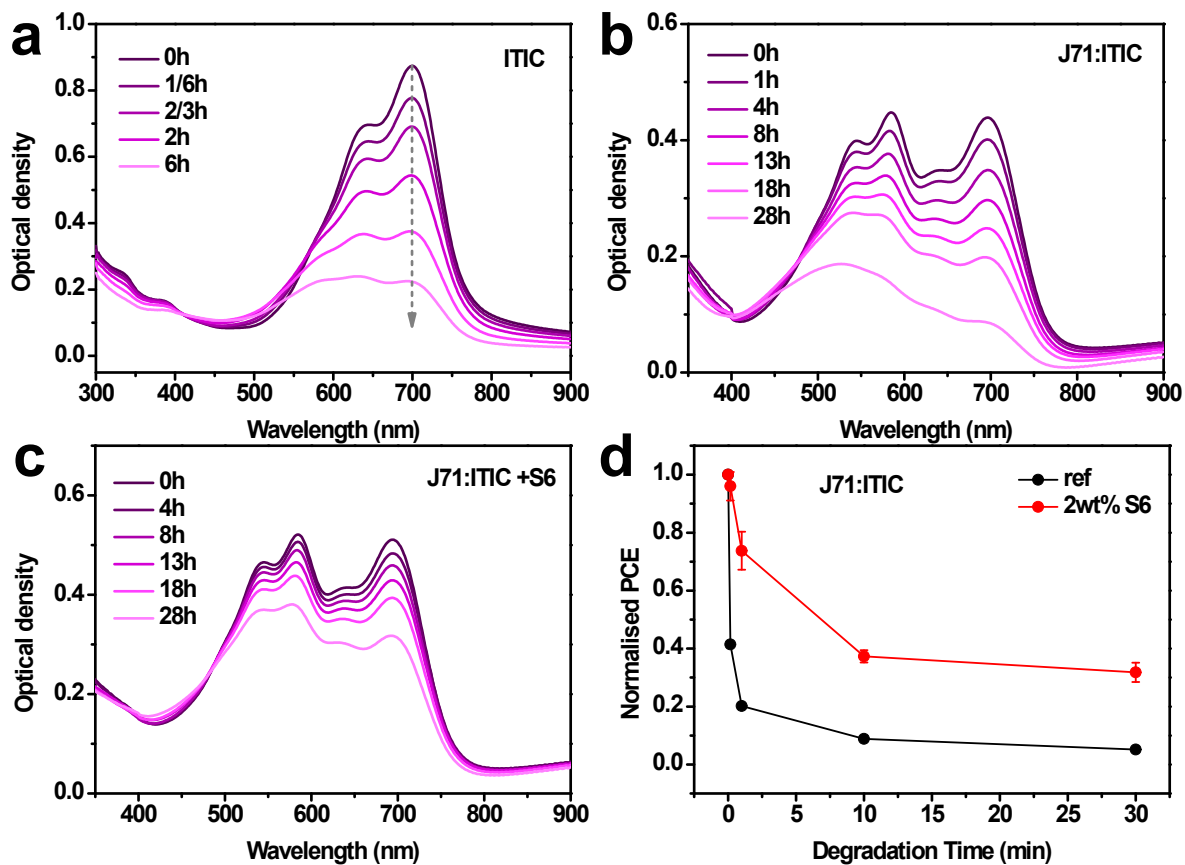


Figure S60. (a-c) Absorption spectra of ITIC, J71:ITIC blends film without and with 2 wt% S6 aged in ambient under 100 mW cm^{-2} illumination. (d) Normalized PCE of ITO/PEDOT:PSS/J71:ITIC/PDINO/Al device with and without S6 as function of time of exposure to solar simulator light prior to back contact deposition..

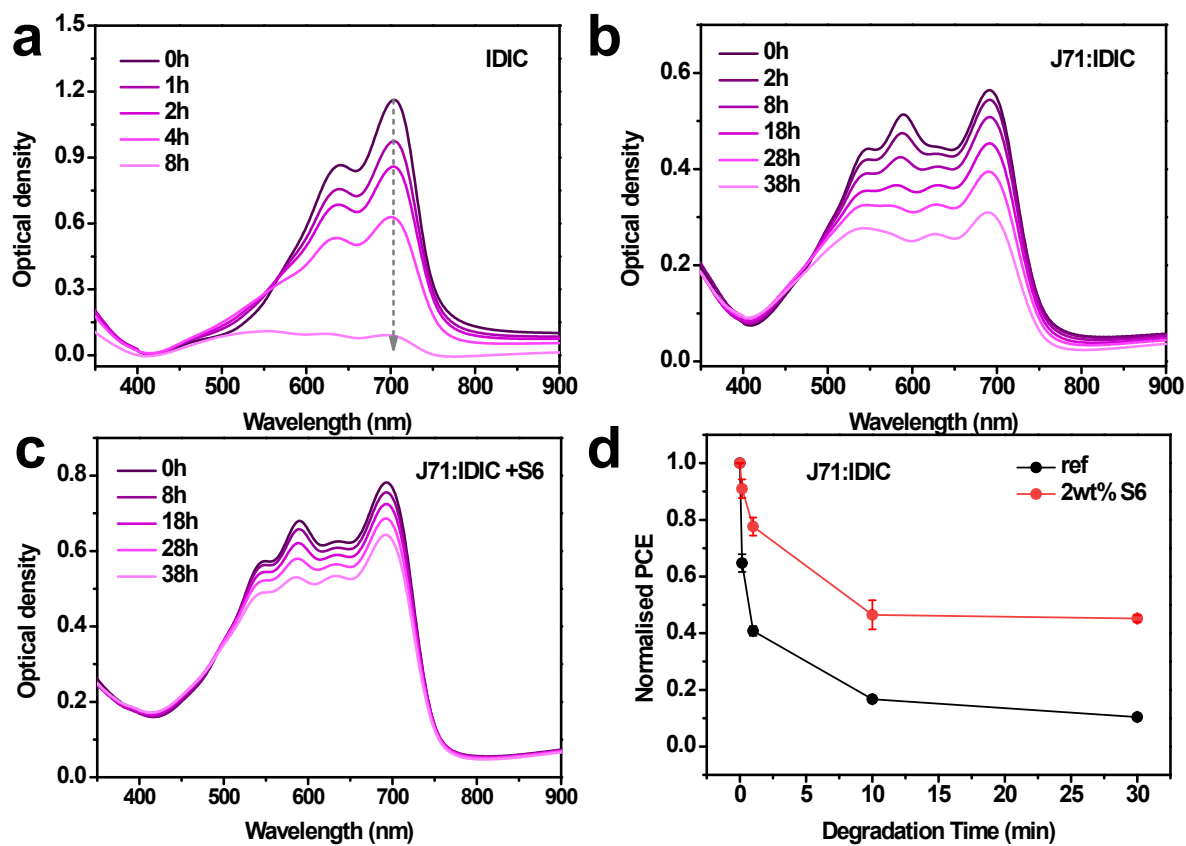


Figure S61. (a-c) Absorption spectra of IDIC, J71:IDIC blends film without and with 2 wt% S6 aged in ambient under 100 mW cm^{-2} illumination. (d) Normalized PCE of ITO/PEDOT:PSS/J71:IDIC/PDINO/Al device with and without S6 as function of time of exposure to solar simulator light prior to back contact deposition.

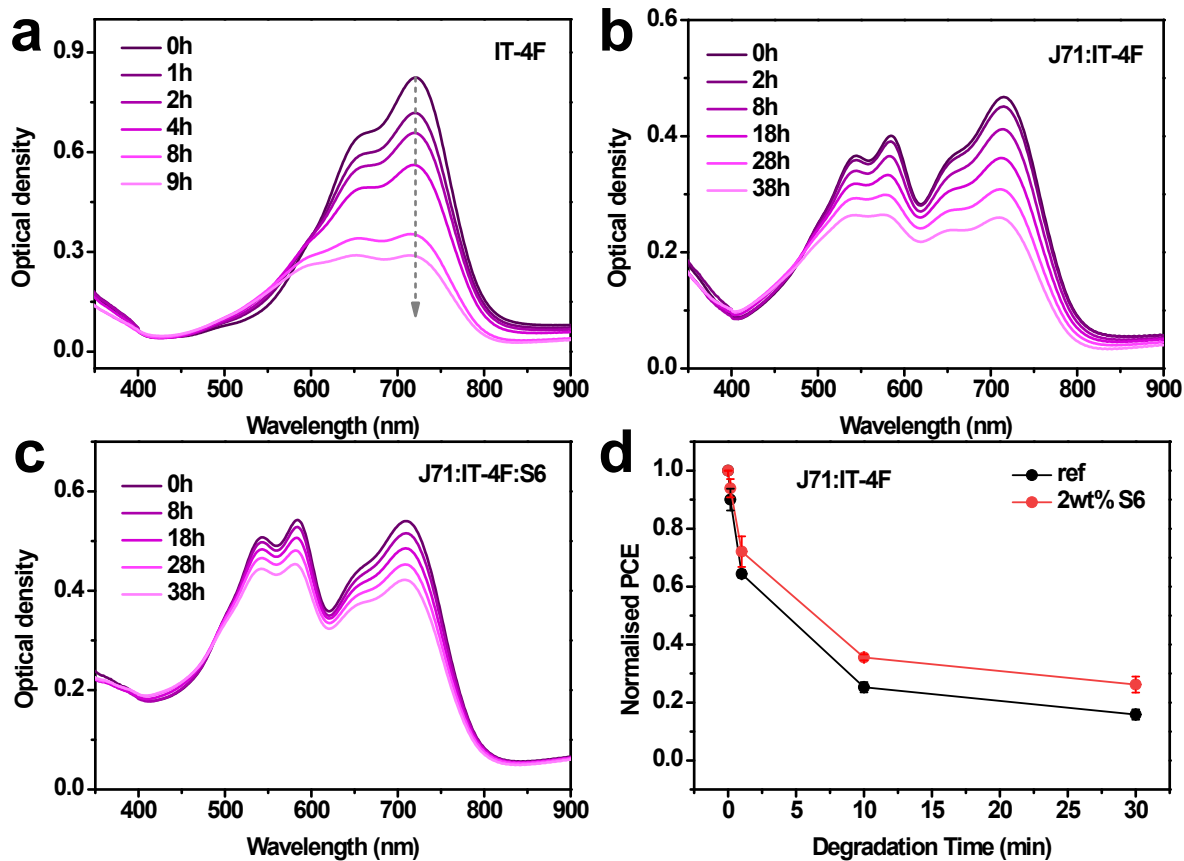


Figure S62. (a-c) Absorption spectra of IT-4F, J71:IT-4F blends film without and with 2 wt% S6 aged in ambient under 100 mW cm^{-2} illumination. (d) Normalized PCE of ITO/PEDOT:PSS/J71:IT-4F/PDINO/Al device with and without S6 as function of time of exposure to solar simulator light prior to back contact deposition.

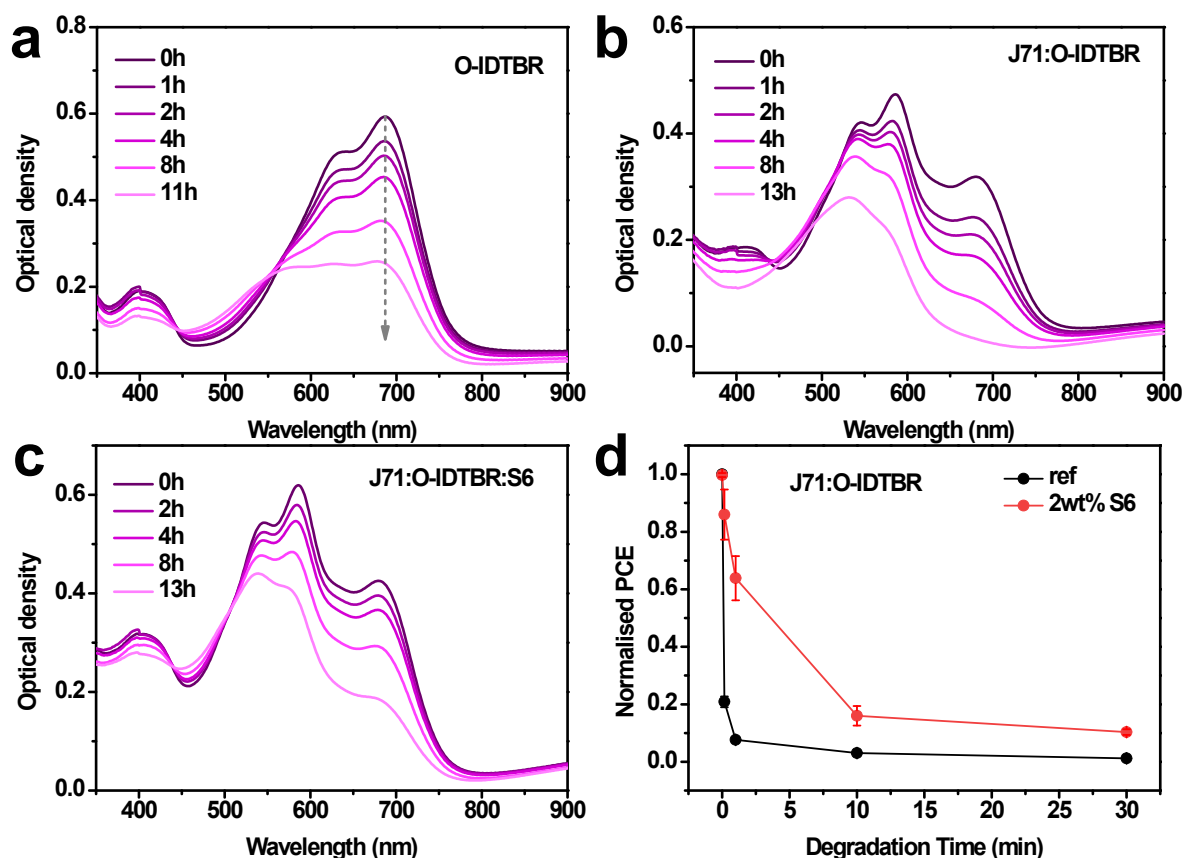


Figure S63. (a-c) Absorption spectra of O-IDTBR, J71:O-IDTBR blends film without and with 2 wt% S6 aged in ambient under 100 mW cm^{-2} illumination. (d) Normalized PCE of ITO/PEDOT:PSS/ J71:IDIC/PDINO/Al device with and without S6 as function of time of exposure to solar simulator light prior to back contact deposition.

Table S6. Summary of device parameters of ITO/PEDOT:PSS/J71:ITIC/PDINO/Al devices with different contents of S6, measured under simulated AM1.5G illumination. The photovoltaic parameters are the average values of six devices.

S6 additives	V_{oc} [V]	J_{sc} [mA/cm ²]	FF [%]	PCE [%]
ref	0.948	15.95	67.21	10.16
0.2 wt%	0.935	15.04	63.06	8.87
0.5 wt%	0.922	14.56	61.22	8.18
1 wt%	0.921	12.17	61.07	6.84
2 wt%	0.913	11.29	58.14	6.00

Reference:

1. Vandewal, K., Tvingstedt, K., Gadisa, A., Inganäs, O. & Manca, J.V. Relating the open-circuit voltage to interface molecular properties of donor: Acceptor bulk heterojunction solar cells. *Physical Review B* **81**, 125204 (2010).
2. Rau, U. Reciprocity relation between photovoltaic quantum efficiency and electroluminescent emission of solar cells. *Physical Review B* **76**, 435 (2007).
3. Shockley, W. & Queisser, H.J. Detailed balance limit of efficiency of p-n junction solar cells. *Journal of Applied Physics* **32**, 510–519 (1961).
4. Liu, J. et al. Fast charge separation in a non-fullerene organic solar cell with a small driving force. *Nature Energy* **1**, 16089 (2016).
5. Luo, Z. et al. Reduced Energy Loss Enabled by a Chlorinated Thiophene-Fused Ending-Group Small Molecular Acceptor for Efficient Nonfullerene Organic Solar Cells with 13.6% Efficiency. *Advanced Energy Materials* **3**, 1900041 (2019).
6. Lin, Y. et al. An electron acceptor challenging fullerenes for efficient polymer solar cells. *Advanced materials* **27**, 1170–1174 (2015).
7. Huang, H. et al. Enhanced open circuit voltage of small molecule acceptors containing angular-shaped indacenodithiophene units for P3HT-based organic solar cells. *Journal of Materials Chemistry C* **6**, 12347–12354 (2018).
8. Li, S. et al. Energy-Level Modulation of Small-Molecule Electron Acceptors to Achieve over 12% Efficiency in Polymer Solar Cells. *Advanced materials* **28**, 9423–9429 (2016).
9. Wang, W. et al. Fused Hexacyclic Nonfullerene Acceptor with Strong Near-Infrared Absorption for Semitransparent Organic Solar Cells with 9.77% Efficiency. *Advanced materials* **29**, 1701308 (2017).
10. Li, T. et al. Fused Tris(thienothiophene)-Based Electron Acceptor with Strong Near-Infrared Absorption for High-Performance As-Cast Solar Cells. *Advanced Materials* **30**, 1705969 (2018).
11. Yao, H. et al. Achieving Highly Efficient Nonfullerene Organic Solar Cells with Improved Intermolecular Interaction and Open-Circuit Voltage. *Advanced materials* **29**, 1700254 (2017).
12. Dai, S. et al. Enhancing the Performance of Polymer Solar Cells via Core Engineering of NIR-Absorbing Electron Acceptors. *Advanced materials* **30**, 1706571 (2018).
13. Zhang, Z. et al. Achieving over 10% efficiency in a new acceptor ITTC and its blends with hexafluoroquinoxaline based polymers. *Journal of Materials Chemistry A* **5**, 11286–11293 (2017).
14. Chen, Y. et al. Modulation of End Groups for Low-Bandgap Nonfullerene Acceptors Enabling High-Performance Organic Solar Cells. *Advanced Energy Materials* **8**, 1801203 (2018).
15. Luo, Z. et al. Asymmetric thieno [2, 3-b] thiophene-based electron acceptor featuring a seven fused-ring electron donor unit as core for nonfullerene organic photovoltaics. *Organic Electronics* **62**, 82–88 (2018).
16. Luo, Z. et al. Fine-Tuning of Molecular Packing and Energy Level through Methyl Substitution Enabling Excellent Small Molecule Acceptors for Nonfullerene Polymer

- Solar Cells with Efficiency up to 12.54%. *Advanced materials* **30**, 1706124 (2018).
17. Xiao, Z. et al. 26 mA cm⁻² Jsc from organic solar cells with a low-bandgap nonfullerene acceptor. *Science Bulletin* **62**, 1494-1496 (2017).
 18. Yuan, J. et al. Fused Benzothiadiazole: A Building Block for n-Type Organic Acceptor to Achieve High-Performance Organic Solar Cells. *Advanced materials* **31**, 1807577 (2019).
 19. Lin, Y. et al. High-Performance Electron Acceptor with Thieryl Side Chains for Organic Photovoltaics. *Journal of the American Chemical Society* **138**, 4955-4961 (2016).
 20. Yuan, J. et al. Single-Junction Organic Solar Cell with over 15% Efficiency Using Fused-Ring Acceptor with Electron-Deficient Core. *Joule* (2019).
 21. Zhao, W. et al. Molecular Optimization Enables over 13% Efficiency in Organic Solar Cells. *Journal of the American Chemical Society* **139**, 7148-7151 (2017).
 22. Sun, J. et al. Dithieno3,2-b:2',3'-dipyrrol Fused Nonfullerene Acceptors Enabling Over 13% Efficiency for Organic Solar Cells. *Advanced materials* **30**, 1707150 (2018).
 23. Zhang, H. et al. Over 14% Efficiency in Organic Solar Cells Enabled by Chlorinated Nonfullerene Small-Molecule Acceptors. *Advanced materials* **30**, 1800613 (2018).
 24. Gong, Y. et al. Pyrene-fused PDI based ternary solar cells: high power conversion efficiency over 10%, and improved device thermal stability. *Materials chemistry frontiers* **3**, 93-102 (2019).
 25. Kan, B. et al. A chlorinated low-bandgap small-molecule acceptor for organic solar cells with 14.1% efficiency and low energy loss. *Science China Chemistry* **61**, 1307-1313 (2018).
 26. Zhang, Z. et al. Conformation Locking on Fused-Ring Electron Acceptor for High-Performance Nonfullerene Organic Solar Cells. *Advanced Functional Materials* **28**, 1705095 (2018).
 27. Lin, Y. et al. A facile planar fused-ring electron acceptor for as-cast polymer solar cells with 8.71% efficiency. *Journal of the American Chemical Society* **138**, 2973-2976 (2016).
 28. Holliday, S. et al. High-efficiency and air-stable P3HT-based polymer solar cells with a new non-fullerene acceptor. *Nature communications* **7**, 11585 (2016).
 29. Qu, J. et al. Chlorine Atoms Induced Molecular Interlocked Network in a Non-Fullerene Acceptor. *ACS applied materials & interfaces* **10**, 39992-34000 (2018).